NASA TECHNICAL NOTE

HIGH-PRESSURE FLAME SYSTEM FOR POLLUTION STUDIES WITH RESULTS FOR METHANE-AIR DIFFUSION FLAMES

Irvin M. Miller and Howard G. Maahs

Langley Research Center
Hampton, Va. 23665

NATIONAL AERONAUTICS AND SPACE ADMINISTRATION • WASHINGTON, D. C. • JUNE 1977

1. Report No.	2. Government Accession No.	
NASA TN D-8407		

4. Title and Subtitle

HIGH-PRESSURE FLAME SYSTEM FOR POLLUTION STUDIES WITH RESULTS FOR METHANE-AIR DIFFUSION FLAMES

June 1977

6. Performing Organization Code

7. Author(s)

Irvin M. Miller and Howard G. Maahs

8. Performing Organization Report No.
L-11199

10. Work Unit No.
505-03-31-01

9. Performing Organization Name and Address

NASA Langley Research Center
Hampton, VA 23665

11. Contract or Grant No.

13. Type of Report and Period Covered
Technical Note

12. Sponsoring Agency Name and Address

National Aeronautics and Space Administration
Washington, DC 20546

14. Sponsoring Agency Code

15. Supplementary Notes

16. Abstract

A high-pressure flame system has been designed and constructed for studying nitrogen oxide formation in fuel-air combustion. Its advantages and limitations have been demonstrated by tests with a confined laminar methane-air diffusion flame over the pressure range from 1 to 50 atm. The methane issued from a 3.06-mm-diameter port concentrically into a stream of air contained within a 20.5-mm-diameter chimney. As the combustion pressure is increased, the flame changes in shape from wide and convex to slender and concave, and there is a marked increase in the amount of luminous carbon. The height of the flame changes only moderately with pressure.

Measured values of average nitric oxide formation rate are greater than those predicted by the conventional two-step Zeldovich mechanism with oxygen atoms assumed to be in equilibrium with oxygen molecules. The molar emission index for NO_X (the moles of total nitrogen oxides formed per mole of methane consumed) increases rapidly as pressure is increased, reaches a maximum at about 9 atm, and thereafter decreases slowly until at 50 atm it has returned to approximately the same value that it was at 1 atm. This maximum occurs in spite of the fact that the peak temperature in the flame decreases as pressure is increased. Unfortunately, the present data are insufficient to permit a clear choice among several alternatives offered for explaining this maximum.

17. Key Words (Suggested by Author(s))	18. Distribution Statement
Pollution Combustion High pressure Nitric oxide formation Diffusion flame	Unclassified - Unlimited Subject Category 25

19. Security Classif. (of this report)	20. Security Classif. (of this page)	21. No. of Pages	22. Price*
Unclassified	Unclassified	75	$4.50

* For sale by the National Technical Information Service, Springfield, Virginia 22161

HIGH-PRESSURE FLAME SYSTEM FOR POLLUTION STUDIES WITH RESULTS FOR METHANE-AIR DIFFUSION FLAMES

Irvin M. Miller and Howard G. Maahs
Langley Research Center

SUMMARY

A high-pressure flame system has been designed and constructed for studying nitrogen oxide formation in fuel-air combustion. Its advantages and limitations have been demonstrated by tests with a confined laminar methane-air diffusion flame over the pressure range from 1 to 50 atm. The methane issued from a 3.06-mm-diameter port concentrically into a stream of air contained within a 20.5-mm-diameter chimney. Except for special studies of flame stability, fuel and air flow rates were held constant at 41.8 standard cm^3/min (sccm) and 2450 sccm, respectively.

As the pressure of the flame was increased from 1 to 50 atm, its shape changed from wide and convex to slender and concave. At the same time, there was a marked increase in the amount of carbon in the flame as evidenced by its greatly increased luminosity. The height of the flame changed moderately with pressure. At higher pressures the limits of stability and extinction were greatly reduced and the limits within which the flame smoked were greatly increased.

Average nitric oxide formation rates were greater than those predicted by the conventional two-step Zeldovich mechanism with oxygen atoms assumed to be in equilibrium with oxygen molecules. Without making the oxygen-atom equilibrium assumption, required superequilibrium oxygen-atom ratios were calculated using the Zeldovich mechanism. At 1 atm, these ratios were close to literature values reported for premixed flames, but they increased markedly above 5 atm. It may be that at elevated pressures an increasing amount of nitric oxide was formed through nitrogen-hydrocarbon reactions in addition to the Zeldovich mechanism.

The molar emission index for NO_x (the moles of total nitrogen oxides formed per mole of methane consumed), which was 0.85×10^{-3} at 1 atm, increased rapidly as pressure was increased; it reached a maximum value of 1.21×10^{-3} at about 9 atm; and thereafter it decreased slowly until at 50 atm it was back to the same value that it was at 1 atm. This maximum occurred in spite of the fact that the peak temperature in the flame decreased from about 2130 K at 1 atm to about 1850 K at 20 atm, and thereafter, at higher pressures, decreased relatively little. Unfortunately, the present data are insufficient to permit a clear choice among several alternate explanations of this maximum offered in this report. A number of experiments which would aid in making such a choice are suggested.

INTRODUCTION

Pollution from aircraft turbine engines is an increasing national concern as more aircraft and more powerful engines are placed into service. The problem is particularly severe in and around airports because of aircraft concentration and the greater quantity of fuel burned on take-off. Of the various pollutants discharged from these engines, two of the most harmful are nitric oxide and nitrogen dioxide, commonly referred to as NO_X. A primary national goal is to control these NO_X emissions, and numerous studies, both experimental and analytical, have been made toward this end.

Experimental studies have involved measurements of pollutants in the combustors and exhausts of turbine engines to correlate engine emissions with parametric adjustments in the combustor. Analytical combustion models have been formulated to predict pollutant formation in a given combustor. Each model consists of a unique combination of assumed chemical and fluid-mechanical mechanisms which is supposed to represent the combustion process. Such models can be of great value for designing more efficient, cleaner combustors if the assumed combination of mechanisms accurately represents the combustion, flow, and pollutant formation processes actually occurring in a given combustor. Since the actual combustion and flow processes are very complex (involving fuel injection, atomization and evaporation, air addition, partial recirculation, diffusion, heat transfer, turbulence, etc., at pressures up to 30 atm), experimental verification is necessary. However, such verification is difficult and very expensive in actual combustors. An alternate approach would be to check combustion models with a simplified laboratory combustion system. To the authors' knowledge, there are no such laboratory combustion systems being used to verify combustion models at high pressures (30 atm and higher).

Within an actual turbine engine combustor, the mixing state of fuel and air can exist locally between two limits: completely unmixed, as in the vicinity of a vaporized fuel droplet near the fuel jet, and completely mixed, as in the highly turbulent region of the combustor. These two localized limiting states can be simulated in the laboratory by either of two simplified combustion systems, the data from which can be useful in verifying current combustion models as well as in furthering the understanding of the NO_X formation process in hydrocarbon flames. These two systems are a laminar diffusion flame and a laminar premixed flame. The laminar diffusion flame was chosen for the initial design and construction of the experimental facility because it is experimentally safer and simpler, and it is not complicated by problems of mixing and flashback which become severe for premixed flames at high pressures.

On the basis of the foregoing considerations, a high-pressure flame system was designed, constructed, and tested to determine the effect of pressure on NO_X emissions from hydrocarbon-air flames. Descriptions of this facility, of the combustion gas analysis system, and of the instrumentation for measuring the temperature of the luminous zone in the flame are presented in the first three sections of this report. Results obtained for a methane-air diffusion flame are presented and discussed in the last two sections.

Certain commercial materials are identified in this report in order to specify adequately which materials were used in the research effort. In no case does such identification imply recommendation or endorsement of the product by NASA, nor does it imply that the materials are necessarily the only ones or the best ones available for the purpose. In many cases equivalent materials are available and would probably produce equivalent results.

SYMBOLS

C_i	molar concentration of species i, moles/cm^3
$\bar{C}_i$	average molar concentration of species i, moles/cm^3
c	mass concentration of carbon, g/cm^3
c_1	first Planck constant, 3.741844 pJ-cm^2/sec
c_2	second Planck constant, 1.438833 cm-K
d_C	average carbon-particle diameter, Å or nm (1 Å = 0.1 nm)
E_λ	Planck function, defined by equation (D7)
$F(\lambda)$	function defined by equation (D3)
I	emission index, (g of NO_X as if all were NO_2)/(kg of CH_4 consumed)
I_m	molar emission index, (moles of NO_X produced)/(mole of CH_4 consumed)
$I_{m,eq}$	molar emission index for NO_X at equilibrium, (moles of NO_X produced)/(mole of CH_4 consumed)
K_0	equilibrium constant defined by equation (10)
K_λ	spectral extinction coefficient, cm^2/g
k	arbitrary constant
k_f, k_r	forward and reverse elementary reaction-rate constants, cm^3/mole-sec (number in subscript (e.g., k_{f6}) refers to equation number)
L	radiation path length, cm
M_i	molecular weight of species i, g/mole
m	complex index of refraction, n - inκ
N_A	Avogadro's number, 6.023 × 10^{23} molecules/mole
N_C	number density of carbon particles, cm^{-3}

$N^{o}_{CH_4}$	number of carbon atoms available in methane fuel per unit volume of reaction zone in flame assuming stoichiometric combustion in flame zone
n	refractive index
$\dot{n}$	molar flow rate, moles/sec
p	pressure, atm (1 atm = 101.3 kPa)
R	universal gas constant, cal/mole-K or cm^3-atm/mole-K
r_i	reaction rate of species i, moles/cm^3-sec
$\bar{r}_i$	average reaction rate of species i, moles/cm^3-sec
S	stoichiometric molar fuel-air ratio
T	temperature, K
T_{ad}	adiabatic flame temperature, K
T_{av}	average temperature in reaction zone, K
$T_{b,\lambda}$	brightness temperature at wavelength λ, K
T_f	peak temperature in flame, K
t	time, sec
$\dot{V}$	volumetric flow rate, cm^3/sec
V_{Rx}	reaction volume, cm^3
w	specific surface reaction rate, moles/cm^2-sec
x_i	mole fraction of species i
$\bar{x}_i$	average mole fraction of species i
$x^{o}_{CH_4}$	mole fraction of methane that would exist in flame zone under stoichiometric conditions if none had been converted to soot
$x^{stoich}_{O,eq}$	equilibrium oxygen-atom mole fraction for stoichiometric premixed combustion
$x_{O,req'd}$	oxygen-atom mole fraction required by equation (8) to give observed NO_X formation rate
α	dispersion exponent; arbitrary constant
β	arbitrary constant

Γ surface area of carbon particles in flame per unit volume of reaction zone in flame

ε_λ spectral emissivity

κ absorption index

λ wavelength, Å or nm (1 Å = 0.1 nm)

ρ_C carbon-particle mass density, g/cm^3

ϕ equivalence ratio

ϕ' pseudoequivalence ratio, defined by equation (1)

χ quantity defined in appendix E

Subscripts:

max maximum value assuming all carbon in fuel has been converted to carbon particles

stoich stoichiometric conditions

STP at standard temperature and pressure, 293 K and 1 atm

Superscripts:

carbon for stoichiometric conditions assuming that all methane has been transformed to carbon and hydrogen

E experimental

stoich for stoichiometric conditions assuming perfect mixing

Chemical symbols:

C carbon atom

C_2 diatomic carbon

CH carbon-hydrogen radical

CH_4 methane

CO carbon monoxide

CO_2 carbon dioxide

H_2 hydrogen molecule

H_2O water

He	helium
M	arbitrary third body
N	nitrogen atom
N_2	nitrogen molecule
NO	nitric oxide
NO_2	nitrogen dioxide
NO_x	total nitrogen oxides (NO and NO_2)
O	oxygen atom
O_2	oxygen molecule
OH	hydroxyl radical

Abbreviations:

C/L-A	chemiluminescent analyzer
cal.	calibration
diam	diameter
F.M.	flowmeter
IR	infrared
i.d.	inside diameter
o.d.	outside diameter
sccm	standard cm^3/min

DESCRIPTION OF SYSTEM

The high-pressure flame system developed for this study represents the first such system for the investigation of confined laminar diffusion flames at elevated pressures up to 50 atm. The confined laminar diffusion flame, first analyzed by Burke and Schumann (ref. 1), is a flame burning at the exit of a tube from which fuel gas issues coaxially into a cylindrical duct of coflowing air (or other oxidizer). An important part of the present high-pressure system is the provision for collection and analysis of the products of combustion from the flame, particularly oxides of nitrogen. The initial design of the system was based on the following parameters:

Fuel	Methane
Molar fuel-air ratio	0.1 to 1.0
Fuel flow rate, sccm	152 maximum
Combustion pressure, atm	1 to 50

Burner Design

The heart of the high-pressure diffusion flame system is the burner, where methane gas (99.97 percent pure) issues coaxially from a cylindrical tube into a concentric cylindrical quartz tube through which air (99.995 percent pure, total hydrocarbon concentration less than 1 ppm) is coflowing, as shown in figure 1. If the air and fuel streams are laminar, then the air and fuel mix largely by diffusion. Under these conditions, a stable diffusion flame results upon ignition. Burke and Schumann (ref. 1) were the first to analyze theoretically this type of flame, and they developed an equation which predicts the flame height and shape for laminar flow. However, they experimentally verified their equation only over the very limited pressure range from 1 to 1.5 atm.

The equation developed by Burke and Schumann (ref. 1) and Reynolds criteria for laminar flow in tubes were used to size the burner for a small luminous flame. In addition to laminar flow requirements, the flame had to be luminous and nonsmoking. A luminous flame was necessary for measuring the temperature of the luminous zone by a relatively simple spectroscopic technique. This technique is discussed in a subsequent section. The requirement that the flame be nonsmoking avoids the problem of contaminating the system as well as of removing soot from the combustion products.

To obtain a smoke-free, luminous flame at 1 atm, the pseudoequivalence ratio ϕ', defined as the actual molar ratio of fuel to air divided by the stoichiometric molar ratio of fuel to air,[1] must be less than 1. If ϕ' is near 1, the flame is luminous and sooty, and if ϕ' is greater than 1, the flame is nonluminous and contains large quantities of unburned hydrocarbons. Examples of these types of flames are shown in figure 2. (Extensive, detailed descriptions of such flames for the butane-air system at 1 atm are given by Barr (ref. 2).) From appendix A, the value of ϕ' can be set by controlling the volumetric flow rates of fuel and air at standard conditions of temperature and pressure (293 K and 1 atm), or

$$\phi' = \frac{1}{S} \frac{\dot{V}_{STP,fuel}}{\dot{V}_{STP,air}} \tag{1}$$

[1]The term "pseudoequivalence ratio" has been coined for the present diffusion flame because the concept of equivalence ratio does not hold the same fundamental significance for a diffusion flame that it does when used for premixed flames. In an overventilated diffusion flame (i.e., $\phi' < 1$) such as the one under study, it is generally assumed that the effective equivalence ratio in the flame zone where the reaction actually occurs is very close to unity.

where S is the stoichiometric fuel-air ratio and $\dot{V}_{STP,fuel}$ and $\dot{V}_{STP,air}$ are the volumetric flow rates of fuel and air at standard conditions. For all measurements, the volumetric flow rates of fuel and air were maintained at 41.8 and 2450 sccm, respectively, for reasons discussed in the section, Smoke, Stability, and Extinction Limits. Under these conditions with S = 0.105 for methane, $\phi' = 0.162$ by equation (1).

The fuel tube has an inside diameter of 3.06 mm and a wall thickness of 0.05 mm. (See fig. 1.) The outlet edge of the tube is tapered to minimize the formation of turbulent eddies. The quartz air tube, hereafter referred to as the quartz chimney, has an inside diameter of 20.5 mm. In order to obtain a flat velocity profile in the fuel and air streams as they exit from the fuel and air ducts (with the intent of simplifying any theoretical analysis of the combustion process in the diffusion flame), a porous disk of sintered stainless steel was installed near the exit of the fuel duct as well as near the exit of the air duct, as shown in figure 1. In preliminary tests, no porous disks were installed in the fuel and air ducts, and it was not possible to sustain a flame after ignition at pressures approaching 50 atm. At these pressures, with the hot-wire igniter located near the fuel duct exit, the flame appeared and disappeared in a cyclic manner - on for a fraction of a second, off for more than a second. However, with porous disks installed in both the fuel and air ducts, a flame, once ignited, was self-sustaining. Other tests with a porous disk only in the fuel duct were partially successful - combustion was sometimes cyclic, other times continuous. Consequently, all subsequent tests employed porous disks in both the fuel and air ducts.

In early tests at pressures above 40 atm, a band of tiny condensate droplets formed on the inside of the chimney, extending from about halfway up the flame to the top of the chimney. This was probably due to the cooling effect of the nitrogen pressurizing gas sweeping past the side of the chimney. This problem was considerably reduced by surrounding the chimney with a larger square quartz chimney. As a result, only a very thin band of condensate formed inside the chimney above the flame, and this soon reached a steady-state amount.

Sample-Handling System

When methane is burned with air, the primary combustion products are carbon dioxide and water vapor, although small quantities of carbon monoxide and NO_x are also formed. To make studies of pollution formation in the flames, a sampling system was devised which collects the total combustion products given off by the flame and transports them to the gas analyzers. A description of the gas analyzers is given in a subsequent section.

A schematic diagram of the sample collection system is shown in figure 3. The hot combustion products from the flame exit from the top of the quartz chimney and are swept upward into an electrically heated total-sample collector by the nitrogen pressurizing gas. The diluted combustion gases continue to flow upward through an electrically heated tube, a hot-air-heated 5-μm particle filter, and a hot-air-heated back-pressure regulator. The filter and regulator are located outside the pressure chamber. At the exit of the back-pressure

regulator, the total gas sample is vented to unheated sample transfer lines at atmospheric pressure and thence to the gas analyzers. All surfaces contacted by the total gas sample, from the chimney exit to the gas analyzers, are of stainless steel.

The purpose of the nitrogen dilution gas is twofold: (1) it serves as the pressurizing gas in the combustion chamber, and (2) it reduces the partial pressure of water vapor in the total sample and hence lowers the saturation temperature of the water vapor in that sample. This makes it possible to maintain all the water produced during combustion in the vapor state by heating the sample transfer lines to only 393 K, even for the highest pressure of 50 atm. For the sample transfer lines downstream of the back-pressure regulator where the sample is at 1 atm, no heating is necessary. (See appendix B.)

Ignition System

Ignition is accomplished by means of an electrical resistance-heated hot-wire igniter. This igniter, shown in figure 4, is retractable through a Chevron packing gland at the top of the sample transfer line in the chamber (see fig. 3). During operation, the igniter is positioned 10 to 20 mm above the burner, and electric power is applied until ignition is attained. Power to the igniter is then shut off and the igniter retracted to the top of the sample transfer line where it is completely out of the sample flow.

Flow and Pressure Control System

A schematic diagram of the flow and pressure control system is shown in figure 5. Gas flows are controlled with micrometer needle valves. The upstream pressure of these valves is controlled by dome-loaded regulators and the downstream pressure or chamber pressure is controlled by a dome-loaded back-pressure regulator. The control pressures for the three dome-loaded regulators and for the back-pressure regulator are provided by two separate spring-loaded regulators. Since the spring-loaded regulators tend to drift, block valves are used to lock in the set pressures. A gas reservoir was installed in each locked-in system to minimize the effect of leaks and changes in ambient temperature.

Pressure in the pressure chamber is measured by two separate Bourdon tube gages. Low pressures from 1 to 8 atm are measured with a gage having a pressure range from 0 to 1.03 MPa (150 psia) and an accuracy of 0.066 percent of full scale. High pressures from 8 to 50 atm are measured with a gage having a pressure range from 0 to 6.89 MPa (1000 psig) and an accuracy of 0.1 percent of full scale. Flow rates of methane, air, and nitrogen are measured with linear thermal mass flowmeters having an accuracy of 1 percent of full scale. Meter ranges were: 0 to 152 sccm for methane, 0 to 3000 sccm for air, and 0 to 50 000 sccm for nitrogen. The methane and air flowmeters were calibrated with a soap-film meter whose calibration is traceable to the National Bureau of Standards. During calibration, appropriate corrections were made for barometric pressure and ambient temperature. Calibrations were made at 1, 25, and 50 atm, the meters being zeroed at each pressure prior to calibration.

Sight Glass Windows

Safety sight glass windows of 66.7-mm viewing diameter are located on opposite sides of the pressure chamber and are made to withstand a pressure of 50 atm. The burner and chimney can be viewed through these windows. Each flange-mounted sight glass consists of two 25-mm-thick quartz plates laminated with a sheet of Teflon (FEP), type A, nominally 0.0381 mm thick, compressed between the plates to a thickness of 0.0127 mm.

Color photographs of the flame were taken through these windows with a 35-mm single-lens reflex camera fitted with a 200 mm/f2.8 reflective lens and with color negative film. Proper exposure of the flame at each pressure was determined by trial and error.

Operation

The high-pressure flame system is operated by setting the desired flows and pressure in the pressure chamber and igniting the flame. The pressure upstream of the micrometer needle flow control valves is first set at a suitable pressure above the desired ambient pressure in the chamber and the flowmeters are zeroed. Then the desired chamber pressure is set with the backpressure regulator and the chamber is pressurized with nitrogen (99.995 percent pure). When the desired chamber pressure is reached, fuel, air, and nitrogen flows are adjusted to their target values: 41.8 sccm for methane, 2450 sccm for air, and about 6000 sccm for nitrogen. (The nitrogen flow rate of 6000 sccm is high enough to prevent condensation in the sample transfer lines but not so high as to dilute excessively the combustion gases to be analyzed. No flame instability was created by the nitrogen flow.) The electrical heaters for the sample transfer lines are energized, and after the sample lines reach the desired temperature, the igniter rod is lowered to a point close to the burner, the flame is ignited, and the igniter rod is withdrawn from the stream of combustion products.

CHEMICAL ANALYSIS

All chemical analyses are made on the total gas mixture exiting from the high-pressure chamber: combustion products, excess air, and pressurizing nitrogen. This overall, or total, gas analysis approach was selected instead of a detailed profile analysis approach for several reasons. First, local composition measurements by probe sampling would have presented severe experimental difficulties since the sample probe and its associated manipulating mechanism must be located entirely within the enclosed high-pressure chamber and actuated remotely. Secondly, reaction zones typically become thinner as pressure is increased, so that there was some question as to whether satisfactory spatially resolved measurements could be obtained in any event. Finally, for these studies, it was believed to be adequate to measure the average pollutant concentration generated by the flame as opposed to measuring detailed concentration profiles throughout the flame.

In early checkout tests with the high-pressure system, all products were analyzed by gas chromatography with the exception of NO_X, which is not amenable to gas chromatographic determination at the low concentrations encountered. The analysis for NO_X was performed with a commercial chemiluminescent NO-NO_X analyzer having a lower limit of detectability of about 0.3 ppb. Chemical analyses from these checkout tests for overventilated flames (the proposed normal operating condition) showed CO to be below the limit of detectability (about 100 ppm) and the total concentration of hydrocarbons was typically about 6 ppm, indicating that combustion was virtually complete to CO_2 and H_2O. When the system was operated at near-stoichiometric flow rates of CH_4 and air, the expected tall smoky flame was encountered. This condition was avoided so as not to deposit soot within the chamber or sample lines. However, several tests were intentionally made on underventilated flames. These showed substantial quantities of CO as well as CO_2, and also substantial quantities of unburned fuel along with four additional hydrocarbons detected by flame ionization. These hydrocarbons were tentatively identified as acetylene, ethylene, ethane, and methanol; however, no attempts were made to make a more positive identification because underventilated flames were not of concern in this study, and in any case, are customarily avoided in most practical combustion systems.

Since these early tests showed that for the proposed normal overventilated operating condition, virtually all the fuel carbon appeared as CO_2, considerable simplification of the analytical system could be made by substituting a continuous infrared CO_2 monitor for the gas chromatograph. Analysis by infrared absorption is not only easier than gas chromatography, but also a continuous record is obtained. The concentration of CO_2 is of particular interest because it provides a means of determining the extent of nitrogen dilution in the pressure chamber independent of measurements of the separate fuel, air, and nitrogen flow rates (these measurements are inherently less accurate). For all subsequent experimental tests, the concentration of CO_2 was determined with a (commercial) infrared analyzer having a repeatability of ±1 percent.

For the measurement of NO and NO_X concentrations, a (commercial) chemiluminescent NO-NO_X analyzer was employed. Corrections for quenching by CO_2 and H_2O in the sample were made according to the factors reported by Maahs (ref. 3). Because of substantial dilution of the combustion products by the pressurizing N_2, these corrections were fairly small, about 2.5 percent. Conversion efficiency of NO_2 to NO in the NO_X catalytic converter (employing a stainless steel coil) was measured frequently and was typically above 98 percent. Appropriate corrections were made for the actual conversion efficiency and are reflected in the total NO_X concentrations.

A schematic diagram of the final gas analysis system is shown in figure 6. The bypass flow around the chemiluminescent analyzer was a convenient means of providing adequate sample flow to the analyzer while at the same time insuring the sample pressure to the analyzer to be 1 atm. This precaution was taken since the chemiluminescent analyzer is mildly sensitive to sample pressure. The flowmeter at the exit of the infrared CO_2 analyzer was installed to monitor the flow rate through the infrared cell, which in effect, is an extremely sensitive way to monitor cell pressure. By maintaining this flow rate constant, constant cell pressure is insured. The other vents and bypass flow lines were

installed as a convenient means of insuring that switching between sample and calibration gases did not disrupt flows in the overall analytical system.

Details of the gas chromatographic system employed in the early checkout tests are given in appendix C. Although sample analyses by gas chromatography were made only in these early tests, the column arrangement and operating conditions might be of some interest to the reader since this gas chromatographic system proved to be not only convenient to use but also permitted an analysis for water and at the same time completely avoided the need for backflushing any of the columns.

FLAME TEMPERATURE MEASUREMENT

The measurement of flame temperature is by far the most difficult, most uncertain, and least satisfactory of any of the measurements made. Measurement of temperature in a flame is inherently difficult, but the poor physical accessibility of the present flame for probing with thermocouples is the main problem. Consequently, optical methods had to be used. Sodium line reversal was ruled out for several reasons. Not only is the technique complicated, but also, no convenient way could be devised to introduce the sodium into the flame without encountering flameout and/or sodium deposition throughout the chamber and sample lines. Furthermore, it was felt best to avoid the introduction of foreign materials (i.e., sodium) if at all possible so as not to perturb the NO_X formation rates. Refractive index methods such as those described by Weinberg (ref. 4) were tried, but distortions caused by the double chimneys and the 5.0-cm-thick quartz windows were too great to permit meaningful analysis.

Considerable effort was expended in attempting to apply the self-absorption method described by Kuhn and Tankin (ref. 5), but without success. In this method, optical techniques are used for determining the absorption coefficients of the carbon particles naturally occurring in the flame. Kuhn and Tankin demonstrated the feasibility of the method for a large (12.5 cm high) luminous propane-air diffusion flame issuing from a 2.5-cm-diameter burner. But for the present, less luminous, much smaller methane flame (about 10 mm high, issuing from a 3.06-mm-diameter burner), the necessary sensitivity could not be obtained to get a reasonable estimate of the carbon-particle absorption coefficients. Another closely related method also attempted is that of Kurlbaum as described by Ribaud, Laure, and Gaudry (ref. 6). It was not successful either, largely for the same reasons.

Only the exceedingly tedious method of OH absorption offered any hope of being able to measure accurately local flame temperatures, and even this method is somewhat uncertain because of the small thickness of the combustion zone in the flame and the consequent high resolution required of an optical system. Therefore, it was decided that a measurement of a spatial average temperature near the hottest point in the flame was the best that was reasonably possible. For this measurement, the method of two-color pyrometry was employed with the naturally occurring carbon in the flame as the radiant emitter. In applying this method, it is assumed that the spectral emissivity of the carbon particles ε_λ can be expressed in the form

$$\varepsilon_\lambda = 1 - e^{-K_\lambda cL} \tag{2}$$

where

$$K_\lambda cL = \frac{kL}{\lambda^\alpha}$$

where k is an arbitrary constant, L is the path length, λ is the wavelength, and α is the dispersion exponent. Since the exponent in the exponential term is typically much smaller than unity for most flames, the exponential term was approximated by the first two terms in a Taylor series expansion, giving $\varepsilon_\lambda \approx kL/\lambda^\alpha$. Then, by using Planck's black-body law and the definition of emissivity, and by making brightness temperature measurements $T_{b,\lambda 1}$ and $T_{b,\lambda 2}$ at two wavelengths λ_1 and λ_2, k can be eliminated and the flame temperature T_f can be expressed by

$$T_f = \frac{\frac{1}{\lambda_1} - \frac{1}{\lambda_2}}{\frac{1}{\lambda_1 T_{b,\lambda 1}} - \frac{1}{\lambda_2 T_{b,\lambda 2}} - \frac{\alpha}{c_2} \ln\left(\frac{\lambda_1}{\lambda_2}\right)} \tag{3}$$

where c_2 is the second Planck constant, 1.438833 cm-K. The only nonmeasured parameter required to calculate flame temperature from this equation is the dispersion exponent α, taken for the present methane-air flames to be 1.4. McAdams (ref. 7) recommends an average value for α of 1.39 for all hydrocarbon flames, while d'Alessio and coworkers (ref. 8) report a value of 1.4 for methane-oxygen flames. However, T_f is actually relatively insensitive to the precise value selected for α. An error analysis of equation (3) using reasonable values for λ_i and $T_{b,\lambda i}$ indicates that a 30-percent uncertainty in α produces only about a 3-percent uncertainty in T_f.

Brightness temperature measurements were made with two disappearing-filament optical pyrometers fitted with interference filters at different wavelengths, nominally 5000 Å and 6500 Å. Since the wavelengths of these filters are known with great accuracy,[2] the largest error in the flame temperatures calculated by equation (3) is due to experimental errors in measuring $T_{b,\lambda i}$. To minimize these errors, as well as the error propagation in equation (3) caused by the wavelengths being too close together, initial tests were made with the pyrometers sighting on a flame through a number of different optical

[2]The 5000-Å filter has a central wavelength of 5002 Å, 63-percent transmission, and 83-Å bandwidth at half-height. The 6500-Å filter has a central wavelength of 6508 Å, 60-percent transmission, and 90-Å bandwidth at half-height.

filters at wavelengths ranging from 4000 Å to 7000 Å. Ultimately, 5000-Å and 6500-Å filters were selected as the best compromise between wavelength separation and eye sensitivity. Both pyrometers were calibrated for brightness temperature as follows: The true temperature of a temperature-controlled black-body cavity was established by a standard optical pyrometer calibrated by the National Bureau of Standards. The pyrometers to be calibrated were then sighted on the black body through the same laminated quartz sight glass window as was used in the chamber and through two thicknesses of quartz glass representing the walls of the two quartz chimneys surrounding the burner. Readings were made on the standard and test pyrometers over a suitable temperature range. For making actual experimental measurements, the pyrometers were attached to adjustable mounts having both vertical and horizontal motion capability and were sighted through the windows in the pressure chamber on the flame at the position of interest. Typically, this position was just below the tip of the flame in the region of the most intense radiation. The experimental pyrometer readings were then converted to standard black-body brightness temperatures by the calibration curves, and flame temperature was calculated from equation (3).

During the course of the experiments, the pyrometer system was improved by incorporating both filters into a single pyrometer with provisions for switching between the two filters. In this way, possible uncertainties in positioning two individual pyrometers when viewing the flame were effectively eliminated.

RESULTS AND DISCUSSION

The high-pressure flame system was successfully operated over the pressure range from 1 to 50 atm. All tests were made with methane as the fuel and air as the oxidizer. Results from these preliminary tests revealed a number of interesting and sometimes unexpected phenomena regarding flame shape, carbon formation, smoke emission, flame stability, extinction limits, NO_x emission levels, and flame temperature. These phenomena are discussed in the following sections.

Flame Shape and Carbon Formation

A very marked change occurred in the shape and structure of the methane-air diffusion flame as pressure was increased from 1 to 50 atm, as illustrated in the color photographs in figure 7. All photographs were taken at the same flow rate of methane (41.8 sccm) and air (2450 sccm), and are shown at an enlargement of about 4.6 to 1. The bottom edge of each photograph in figure 7 is coincident with the top edge of the burner, and the lateral position of the burner is shown below each photograph. At 1 atm, the sides of the flame bow outward from the inner fuel core into the surrounding air annulus, with the result that the diameter of the flame is considerably larger than the diameter of the fuel tube. The blue zone in the photographs is likely due to O_2 Schumann-Runge radiation and CO + O continuum radiation (see Gaydon and Wolfhard (ref. 9)), and the brighter blue-green or green zones on the sides and near the base of the flame are likely due to C_2 and CH radiation (ref. 9). A zone of

weak carbon-particle luminosity is evidenced by the off-white zone in the upper portion of the flame. As pressure was increased above 1 atm, the outward bowing of the sides of the flame continually decreased. The most notable change in shape occurred below about 5 atm. At about 10 atm the flame exhibited a slight concavity and the diameter decreased considerably. Also, the zones of molecular radiation became narrower and did not extend as high; the carbon zone became yellower and much brighter. A further decrease in flame diameter continued as pressure was increased above 10 atm; however, most of the change in shape and structure occurred when 20 atm was reached. At higher pressures up to 50 atm, only minor changes occurred. It seems likely that a change in reaction mechanism with increasing pressure, as evidenced by the presence of increasing amounts of carbon (a reaction intermediate) in the flame, is largely responsible for the pronounced change in shape of the flame. Because of their relatively high mass, solid carbon particles, once formed, do not diffuse outward from the gaseous fuel core as does the gaseous fuel itself, and combustion must proceed by virtue of the fact that oxygen diffuses inward to the carbon zone. Hence, the flame assumes its constricted appearance.

Interestingly, the height of the flame did not change drastically, at least up to about 30 atm, although a rather marked change occurred in the shape of the flame with pressure. A plot of flame height as a function of pressure is shown in figure 8, where the flame heights were determined from the color photographs in figure 7. The height to the tip of the observable blue reaction zone and the height to the tip of the luminous carbon zone are separately indicated for pressures at which they differ. On the basis of the position of the luminous tip, there is roughly a 25-percent increase in the flame height between 1 and 10 atm, and on the basis of overall height, a decrease of about 10 percent. Above 10 atm, the flame height decreases slowly up to about 30 atm; then it drops more steeply to its lowest value at 50 atm. With the exception of 50-atm flames, the flame height was typically 10 mm.

These flame height data in figure 8 conflict with theoretical predictions that the height of a confined laminar diffusion flame should be independent of pressure at constant mass flow both for equal fuel and air velocities (see refs. 1 and 10) and for unequal fuel and air velocities (see refs. 11 and 12). Experimental verification of these theoretical predictions has been previously demonstrated only at very low pressures from 0.06 atm to 1.5 atm. In contrast, Parker and Wolfhard (ref. 13) experimentally showed for acetylene that independence of flame height with pressure at constant mass flow is true only for very small flames; for larger flames the height is independent of pressure only in those situations where diffusion is not the sole rate-limiting process. Larger flames were stated to increase in height as pressure increases, particularly when carbon is formed in the flame. Differing somewhat from these observations in reference 13 are the theoretical predictions of Powell (ref. 14) for a "sandwich burner," which consisted of a row of alternating fuel and air slots. For constant mass flow and for pressures at which diffusion is controlling, Powell predicts flame height to be independent of pressure; but at very low pressures at which reaction rate is controlling, he predicts flame height to vary inversely with pressure. None of these predictions adequately describe the observed change in flame height of the present methane-air flame over the entire pressure range from 1 to 50 atm. But none of the theoretical predictions

account for carbon formation in the flame either, and it is believed that this increasing amount of carbon formed with increasing pressure is largely responsible for the experimental disagreement with theoretical predictions.

In addition to their prediction of the independence of flame height with pressure, Burke and Schumann (ref. 1) similarly predict that the shape of the flame should be independent of pressure. This is obviously not indicated by the present high-pressure results, nor even by low-pressure results. (See refs. 11, 12, and 13.) However, an accurate prediction of flame shape may be too much to expect from the admittedly simple theory of Burke and Schumann which employs many assumptions including those of constant properties (implying, among other things, no buoyancy forces), infinite reaction rate, and no carbon formation; that the theory predicts flame heights as well as it does for small changes in pressure is indeed remarkable.

The observed increase in carbon formation with increasing pressure in a diffusion flame is a well-known phenomenon. (See the literature review of McArragher and Tan (ref. 15).) At 1 atm, very little carbon is formed as indicated by the very low carbon luminosity of the flame. (See fig. 7.) As pressure increases, the amount of carbon formed increases considerably to produce a brilliant incandescent flame. The brightness of these higher pressure flames cannot be appreciated from the photographs in figure 7, since camera exposure time had to be reduced considerably from 3 sec at 1 atm to 0.0005 sec at 50 atm so as not to overexpose the film. Some idea of this increase in luminosity can be seen from figure 9 where measurements of brightness temperature at 6500 Å made in the tip of the flame have been converted to monochromatic emissive power at 6500 Å by Planck's law and are plotted against pressure. The fuel and air flow rates were maintained at the low constant levels mentioned previously to avoid unoxidized carbon (or soot) from being liberated from the flame as smoke at any of the test pressures from 1 to 50 atm.

Figure 7 shows that carbon formation (as evidenced by the white or yellow luminous zone) occurs mainly in the tip of the flame at low pressures, and as pressure is increased, the carbon zone moves downward to fill an increasingly larger portion of the flame. A rough estimate of the actual mass concentration c of carbon in the tip of the flame can be obtained from experimental data on brightness temperature and a knowledge of the flame temperature itself (presented subsequently in this report). Details of the calculation are given in appendix D. The mass concentration of carbon in the flame is shown in figure 10 as a function of pressure. Carbon concentration increases roughly 3 orders of magnitude from 2.5 atm to 20 atm, and above that, not much further increase occurs. In appendix D, the relationship between the number density of carbon particles N_C and the mass concentration c is also derived. If reasonable values of average particle diameter d_C are assumed to be on the order of 50 Å to 100 Å (5 nm to 10 nm) (see Narasimhan and Foster (ref. 16)), then curves of particle number density as a function of pressure can be constructed, as shown in figure 11. To obtain a rough estimate of particle number density for a 1-atm flame, the particle number density curve for 50-Å-diameter particles in figure 11 was extrapolated from 2.5 atm down to 1 atm to what appears to be a reasonable, though admittedly arbitrary, value of 10^8 particles/cm^3. Figure 11 illustrates that by far most of the increase in carbon-particle number

density occurs between 1 and 5 atm, which is in agreement with what would be surmised intuitively from the photographs in figure 7. Above 5 atm, there is more than an order of magnitude increase in particle number density up to about 20 atm, above which the number density changes relatively little on up to a pressure of 50 atm. This phenomenon of increasing carbon concentration with increasing pressure is of particular concern because it clearly indicates that the mechanism of hydrocarbon oxidation at high pressures in diffusion flames is markedly different from that at low pressures. Hence any mathematical description of the diffusional combustion of methane (or any other hydrocarbon, for that matter) with air at pressures even moderately above 1 atm, must properly account for the formation and subsequent combustion of carbon particles in the flame.

Smoke, Stability, and Extinction Limits

Similar to carbon formation, smoke formation also increased with increasing pressure. The terms "carbon" and "smoke" are used here to distinguish between carbon particles within the flame (as evidenced by flame luminosity) and uncombusted carbon particles liberated from the flame. It was possible at 1 atm to burn methane at a fairly high flow rate, producing a large smokeless incandescent flame, but a small increase in pressure transformed this smokeless flame into a quite smoky one. Also, at higher pressures, the limits of stable combustion were considerably reduced. To define more clearly these regions of smoke and stable combustion, a limited series of tests were made at 1, 5, 20, and 50 atm for the present methane-air diffusion flame over a wide range of fuel and air flow rates. The results are shown in figure 12. The main purpose of these tests was to determine regions of extinction and stable combustion, with a secondary purpose of locating luminous and nonluminous regions and smoke boundaries. The upper limits of 152 sccm for methane flow rate and 3000 sccm for air flow rate in figure 12 were dictated by the upper limits of the flowmeters used. No attempt was made in these studies to produce an extensively detailed map of flame shape and extinction such as that produced by Barr (ref. 2) for a butane-air flame; the boundaries indicated in figure 12 are approximate only.

A number of pertinent observations can be made from figure 12. Perhaps the most striking of these is that the limits of combustion are considerably reduced as pressure is increased; in other words, at higher pressures the flow rate ranges of methane and air over which combustion can be maintained are much smaller than those at lower pressures. It was also noted that extinction of a flame burning at high pressures was often abrupt, whereas at lower pressures considerable flickering and instability occurred in a flame burning near its extinction limit. This is believed to be related to the fact that reaction rate increases as the pressure increases, while diffusion rate remains relatively constant with pressure; consequently, the reaction zone becomes thinner. The higher pressure flames, with their characteristically thin reaction zones, are apparently more susceptible to a sudden extinction by a slight perturbation because the reactants cannot be transported into the thin reaction zone fast enough to reestablish a flame which is burning under marginal conditions. At lower pressures, slight perturbations on the flame tend to create only flickering and instability because the transport of reactants is sufficiently fast relative to the reaction rate to bring reactants into proximity of the thicker

reaction zone. Sufficient combustion is thus maintained somewhere within the zone, and the flame reignites itself throughout the reaction zone in bursts.

Figure 12 also shows that the region of stable combustion is markedly reduced as pressure is increased. For the present purposes, stable combustion was taken to be indicated by a virtually motionless flame without any flickering, wavering, pulsating, or other transient phenomena. At 1 atm the flame is everywhere stable within the combustion boundaries shown, except at low fuel flow rates near the transition boundary between an overventilated and underventilated flame. At 5 atm (fig. 12(b)) the region of stable combustion is already reduced considerably in size and occurs only at relatively small fuel flow rates. At 50 atm the stable region is very small indeed (fig. 12(d)), and regardless of flow rate, all flames at 50 atm were found to be luminous. Even at only 20 atm, a nonluminous flame could be produced only in a very limited region of low fuel and air flow rates.

On the basis of figure 12, the fuel flow rate of 41.8 sccm and air flow rate of 2450 sccm used in the preliminary pollution studies in this report were selected as a reasonable compromise between a sufficiently large and yet reasonably stable flame. However, in later studies at these flow rates, an anomalous zone of instability was encountered in the pressure range from about 9 to 16 atm. At these pressures, the flame tip pulsed or bounced vertically up and down but without any perceptible lateral motion. This bouncing of the flame tip is not believed to be caused by the controlling action of the back-pressure regulator because flame stability was reestablished at higher pressures; above 15 atm, and particularly at about 20 atm, the flame was once again very stable, completely devoid of motion, and quite majestic in its slender brilliant appearance. This region of stability persisted up to about 35 or 40 atm, above which a second type of instability sometimes occurred in the tip of the flame. This instability, which was more noticeable at 50 atm and is indicated in figure 12(d), consisted of the upper portion of the flame swaying slowly from side to side. This swaying motion was not large, perhaps less than 1 mm, and was unaccompanied by vertical motion. It is possible that this instability is hydrodynamic, as proposed by Powell and Browne (ref. 17). At such high pressures, strong density gradients exist in the flame because of the very thin reaction zone and its accompanying steep concentration and temperature gradients. Such gradients were particularly obvious just above the flame, even with the unaided eye, from the strong refractive index gradients appearing about one full flame height above the flame. Since these steep density gradients, and their necessarily associated steep velocity gradients, undoubtedly occur within the flame as well, it is not unreasonable to suspect that these gradients may be responsible for the observed flame instability.

Oxides of Nitrogen

After sufficient experience had been gained in operating the high-pressure flame system, experimental tests were made over the entire pressure range from 1 to 50 atm to determine the effect of pressure on the formation of NO_X. All these tests were made with methane as the fuel and air as the oxidizer. A

single flow condition, 41.8 sccm for fuel and 2450 sccm for air,[3] was studied for the reasons mentioned in the previous section. During the tests the stainless steel filter ahead of the back-pressure regulator was removed periodically and inspected for soot accumulation. None was observed because the experimental conditions were selected so that virtually no free soot, or smoke, was liberated from the flame during a test. In those few instances when the flame was inadvertently ignited at too high a fuel flow rate and smoke was generated, the test was aborted and the filter was replaced. For all tests the filters employed had been precleaned ultrasonically with freon and oven-dried for 2 days at 423 K to remove any traces of oil or contamination in the filters.

Results of these experimental tests are shown in figure 13 as molar emission index of NO_X, I_m, as a function of pressure. The molar emission index of NO_X is defined as the number of moles of NO_X (combined total concentrations of NO and NO_2) produced per mole of fuel burned. Experimentally, it was obtained from the ratio of the measured concentrations of NO_X and CO_2 in the effluent from the high-pressure chamber. The molar emission index is analogous to the emission index I customarily used to report data on gas turbine engines. The emission index is defined as the number of grams of NO_X produced, as if all were present as NO_2, per kilogram of fuel burned. According to these definitions, then, the emission index for methane is 2875 times the molar emission index. The data points shown in figure 13 for any given pressure were taken on separate days and indicate a remarkable degree of reproducibility. Figure 13 shows that the molar emission index which is 0.85×10^{-3} at 1 atm increases rapidly as pressure is increased with a maximum value of 1.21×10^{-3} being reached at about 9 atm; above this pressure the molar emission index decreases slowly and continuously until at 50 atm it is back to roughly the same value that it was at 1 atm. Particularly significant for gas turbine engine applications is that for all pressures above 1 atm and approaching 50 atm, the molar emission index is greater than at 1 atm. Limited tests at a few selected pressures in which the flow rate of methane was intentionally varied showed little effect on I_m over the methane flow rate range from 37.6 sccm to 47.9 sccm. No attempts were made to take data at subatmospheric pressures.

A molar emission index for NO is not reported since little could be learned from such a quantity; much of the NO formed in the combustion process is oxidized to NO_2 in the postflame gases and in the sample lines leading to the chemiluminescent analyzer. Because total oxides of nitrogen are conserved both in sampling and in analysis by chemiluminescence in lean flames (ref. 18), the reported concentration of NO_X is an accurate indication of the sum of the concentrations of NO and NO_2 formed during the combustion process. In any event, it is the total oxides of nitrogen which are of interest, and it is these total oxides which are reflected by the molar emission index for NO_X presented in figure 13.

Literature data on NO_X emissions as a function of pressure during combustion are limited, both in the number of studies and in the pressure range covered. Nevertheless, several such studies were located, three for gas turbine

[3]These flow rates yield a pseudoequivalence ratio ϕ' of 0.162.

combustors, and one for an opposed-jet burner. It is important to recognize that although all these studies are for diffusion flames, they are for highly turbulent systems with geometry, fuels, and inlet conditions markedly different from those in the present study. However, the basic trend of the data from these studies is of some interest in comparison with the present results. This comparison is shown in figure 14. Since three of these studies are for gas turbines or gas turbine combustors with the results reported as emission index (I), the present data were converted to emission index for direct comparison. The data for these gas turbine combustor studies in figure 14 are plotted against combustor inlet air pressure over the actual pressure range of the experimental data. These studies are (1) Diehl and Holdeman (ref. 19) for (liquid) Jet-A fuel in a JT8D-9 engine combustor system with constant combustor inlet air temperature of about 659 K, (2) Norgren and Ingebo (ref. 20) for (gaseous) propane fuel in a test combustor with a constant combustor inlet air temperature of 589 K, and (3) Quigg (ref. 21) for a typical liquid jet fuel in an experimental combustor with constant inlet air temperature of about 530 K. The air temperatures in these turbine studies were considerably above the inlet air temperature for the present methane data, which was only about 295 K. From figure 14, the trend of increasing emission index with increasing inlet air temperature is apparent. A line of slope 1/2 has been drawn in figure 14 for reference purposes, since it is commonly assumed (see, for instance, ref. 22) that the NO_X emission index in gas turbine combustors correlates as $p^{1/2}$.

The results of Quigg (ref. 21) are particularly interesting from two points of view. First, they are similar to the present methane data in that they exhibit a maximum in the emission index as a function of pressure, and secondly, they are representative of data for a wide variety of liquid hydrocarbons. Quigg conducted an extensive parametric study in a test combustor for a wide variety of pure liquid hydrocarbons along with JP-5 jet fuel for comparison. Included in his parametric study were variations in combustor inlet air temperature and humidity, combustor pressure, heat input, reference velocity, and method of fuel injection. Regression equations empirically relating emission index to the various combustor operating parameters were then formulated. For all fuels, with all operating parameters constant except pressure, these regression equations are of the form

$$\log_{10} I_{NO_X} = \alpha + \beta p - 0.0016p^2$$

where the precise values of α and β are determined by the values of the various operating parameters and p is the combustor inlet pressure in atmospheres. Typical values for α and β are on the order of 0.60 and 0.042, respectively; these values were used in generating the curve labeled "Quigg (ref. 21)" in figure 14.

The dashed curve in figure 14 labeled "smoky" is from Norgren and Ingebo (ref. 20) for a mixture of ASTM A-1 (liquid) jet fuel and (gaseous) propane in a different nozzle system from that employed for the propane data shown. Mixing was very poor in this nozzle system, and the large amount of smoke produced indicated an overly rich local condition in the primary zone of the combustor. The maximum in this curve is obvious.

In these comparisons of turbine combustor data with the present laminar diffusion flame data (fig. 14), only the shape of the curve, that is, the influence of pressure on NO_x formation, is of significance. The absolute magnitude of the emission index depends on a large number of additional factors, for example, the fuels used and the operating conditions in a gas turbine combustor as compared with a laminar diffusion flame. However, the fact that maxima have also been observed in the combustion of hydrocarbons in gas turbine combustors as well as in the present laminar diffusion flame suggests that this phenomenon is worthy of further study.

The effect of pressure on NO_x formation has also been studied in flames other than those of hydrocarbon fuels. In an early study by Newitt and Lamont (ref. 23), NO_x formation was measured during combustion of CO in artificial atmospheres of O_2/N_2 over the pressure range from 10 to 100 atm in an opposed-jet diffusion flame. (The purpose of this study was to determine whether increased pressure could be effectively employed to produce NO efficiently.) Some of the data of reference 23 have been abstracted for $\phi' = 0.5$, and these are shown in figure 14 for three different supporting atmospheres of O_2/N_2. The emission index for these CO flames, even in an atmosphere of composition fairly close to that of air (33.3 percent O_2/66.6 percent N_2), is more than an order of magnitude greater than the emission index measured for methane in the present study. This is likely due to the fact that CO flames have much higher adiabatic flame temperatures than CH_4 flames, about 225 K higher (ref. 24), and the radiation loss from CO flames should be the same or less than that from CH_4 flames. In contrast to the hydrocarbon data previously discussed, the emission index for CO flames in figure 14 shows no tendency to reach a maximum, at least below 100 atm. Several important differences between CO flames and hydrocarbon flames are the higher flame temperature for CO flames and the fact that no hydrocarbon radicals are present and no carbon is formed in CO flames. Regarding this latter point, note the similarity between the gas turbine combustor data in figure 14 labeled "smoky" and the present methane diffusion flame data; both show an obvious peak in the emission index curve as a function of pressure, and both have a high degree of carbon formation.

Certainly, any attempt to explain the maximum in the NO_x molar emission index curves in figures 13 and 14 cannot ignore the influence of temperature because of the known strong temperature dependence of the NO-forming reactions. However, in light of the experimental temperature data presented in the following section, changes in flame temperature with pressure cannot be used to explain the shapes of these curves.

Flame Temperature

Estimates of the flame temperature were obtained from measurements of brightness temperature at 5000 Å and 6500 Å as discussed previously. It should be recognized that the flame temperatures measured by this technique are really average carbon temperatures, that is, spatial average temperatures of the hot carbon particles existing in the flame in the zone viewed with the optical pyrometer(s). It has been shown by Kuhn and Tankin (ref. 5) in their work with a large propane diffusion flame that the temperature of these carbon particles

is, in fact, a good indication of the true temperature of the flame gases in the vicinity of the carbon particles. But their results also indicate that the peak temperature reached in the flame may be as much as 100 K higher than that in the carbon zone. However, all their work was done at 1 atm where a separation of the carbon zone from the (blue) gaseous reaction zone must undoubtedly exist (they did not show color photographs of their flames such as those in fig. 7). Because of the much lower carbon-forming tendency of the small methane flames in the present study, no meaningful temperature measurements could be made at pressures below 5 atm; and by the time this pressure was reached, the concentration of carbon in the flame had dramatically increased, the reaction zone had become thinner and more condensed, and the separate blue zone was no longer evident. (See fig. 7.) Hence, it may be assumed that no significant separate gaseous reaction zone exists and that all important combustion reactions occur simultaneously within the visible luminous carbon zone. Since flame temperature was measured in the tip of the flame in the region of most intense radiation, this measured temperature may be taken as a reasonable representation of the peak temperature occurring in the flame.

Figure 15 shows a plot of the measured flame temperature T_f as a function of pressure with data limits at each pressure indicated by a vertical line. The fairly broad limits are caused by the high sensitivity of the flame temperature, calculated by equation (3), to small changes in the two individually measured brightness temperatures at the relatively close wavelengths, 5000 Å and 6500 Å. Although a wider separation between the two wavelengths would be desirable to minimize errors, wider separation cannot be conveniently achieved because the relationship $\varepsilon_\lambda \propto k/\lambda^\alpha$ has only been shown to apply in the visible region. An estimate of the flame temperature at pressures below 5 atm was obtained by extrapolating the temperature curve to a value at 1 atm arbitrarily taken to be 100 K below the adiabatic flame temperature of 2230 K to account for molecular radiation and radiation from the small amount of carbon in the flame. This value of 2130 K is in agreement with the maximum value of 2116 K calculated from thermocouple probe data reported by Tuteja (ref. 25)[4] for large, 1-atm methane-air diffusion flames. For comparison, the adiabatic flame temperature T_{ad} for methane-air combustion at stoichiometric conditions has also been plotted in figure 15.

Figure 15 shows that the measured temperature T_f decreases about 160 K from 1 atm to 5 atm, while carbon concentration, and hence radiation from the flame, substantially increases. There is a further decrease of about 120 K from 5 atm to 20 atm as carbon concentration continues to increase. (See figs. 7 and 10.) From 20 atm to 50 atm, only a 50-K decrease in temperature takes place. There is little similarity between the shape of this temperature

[4]Tuteja reports a maximum thermocouple temperature of about 1978 K (3100° F) uncorrected for thermocouple radiation losses. Using standard radiation thermocouple corrections (ref. 26) and the usually accepted value of 0.25 for thermocouple emissivity (see, for instance, refs. 27 and 28) result in a maximum corrected flame temperature of 2116 K. It may be observed that Tuteja himself uses an excessively large emissivity, 0.40, which yields a maximum flame temperature only 20 K below the adiabatic flame temperature.

curve and the shape of the curve of molar emission index in figure 13. At pressures just above 1 atm, molar emission index increases rapidly while temperature decreases; near 9 atm, molar emission index peaks while temperature decreases smoothly; and above about 20 atm, molar emission index continually decreases while temperature decreases only slightly. Hence, it is clear that the shape of the temperature curve with pressure cannot explain by itself the shape of the curve of molar emission index with pressure. Possible explanations for the shape of this molar emission index curve are explored in some detail in the following section.

INTERPRETATION OF NO_X DATA

The fact that the molar emission index for NO_X for the present methane-air diffusion flame attains a maximum as a function of pressure and the fact that the direction of change of molar emission index with pressure is, in general, contrary to the direction of change of temperature with pressure are unusual results and warrant further consideration. In this section, experimental average rate of formation of NO_X is estimated and compared with rates predicted for a variety of different conditions by the conventional two-step Zeldovich mechanism for NO formation. The experimentally observed peak in the curve of molar emission index as a function of pressure is discussed, and several possible explanations are offered.

Rate of Formation of NO_X

An expression for the average rate of formation of NO_X in the flame can be obtained from the definition of molar emission index I_m. Defined as the number of moles of NO_X produced per mole of fuel consumed, the molar emission index can, under conditions of steady state and complete combustion of the fuel (methane), be expressed as

$$I_m = \frac{\dot{n}_{NO_X}}{\dot{n}_{CH_4}}$$

where $\dot{n}_{CH_4}$ is the molar flow rate of CH_4 into the flame and $\dot{n}_{NO_X}$ is the molar flow rate of NO_X out of the flame. Rearranging this expression and dividing by a reaction volume V_{Rx} yields

$$\frac{\dot{n}_{NO_X}}{V_{Rx}} = I_m \frac{\dot{n}_{CH_4}}{V_{Rx}}$$

If the not unreasonable assumption is made that the reaction volume in which NO_X is formed is approximately equal to (though not necessarily coincident with)

the reaction volume in which CH_4 is combusted to CO_2 and H_2O,[5] this equation can be rewritten as

$$\bar{r}^{E}_{NO_X} = I_m \bar{r}^{E}_{CH_4} \tag{4}$$

where $\bar{r}^{E}_{NO_X}$ is the average rate of formation of NO_X within the reaction volume in which it is formed and $\bar{r}^{E}_{CH_4}$ is the average overall rate of conversion of CH_4 to CO_2 and H_2O within the reaction volume in which such conversion occurs. The reaction rate $\bar{r}^{E}_{CH_4}$ can be obtained by dividing the known molar flow rate of methane $\dot{n}_{CH_4}$ by the volume of the flame zone, which can be obtained from the color photographs of the flame in figure 7. Reaction volumes obtained from these photographs should be a fairly accurate measure of the overall fuel consumption volumes since it has been experimentally demonstrated that methane combustion is complete within the flame (i.e., there are no significant quantities of unburned hydrocarbons, CO, or smoke liberated from the flame). Hence, the average methane reaction rate so determined should be a fairly realistic estimate of the true average overall rate of consumption of methane in the flame.

In defining an appropriate methane reaction volume V_{Rx} from the photographs in figure 7, both the blue and the luminous carbon zones must be included because no distinction should be drawn between methane consumption entirely in the gas phase and methane consumption when (solid) carbon is formed as a reaction intermediate; that is, there is no fundamental difference in the concept of reaction volume in which methane is consumed whether the path be

$$CH_4 + 2O_2 \rightarrow \underset{\text{intermediates}}{\text{Gaseous reaction}} \rightarrow CO_2 + 2H_2O$$

or

$$CH_4 + 2O_2 \rightarrow \underset{\text{intermediates}}{\text{Gaseous reaction}} + \underset{\text{intermediates}}{\text{Solid reaction}} \rightarrow CO_2 + 2H_2O$$

Prior to using the photographs in figure 7 for obtaining estimates of such reaction volumes, however, it had to be ascertained whether all zones of

---

[5]Certainly it is reasonable to assume that the volume in which NO_X is formed is roughly proportional to the volume in which CH_4 is consumed. It is considered unlikely that the constant of proportionality would be much less than 1/2 or much greater than 2; hence, for purposes of convenience, it has been taken to be unity. In any event, the precise value selected for this proportionality constant within these bounds has no material effect on the subsequent discussion.

significant reaction could be seen in these photographs. In separate experiments, photographs were taken of the flame from 1 to 50 atm through interference filters at two wavelengths: 3100 Å where OH band emission occurs and 8700 Å where only continuum emission from carbon particles is expected. On comparing these photographs with the color photographs in figure 7, it was found that the photographs taken with the 3100-Å filter coincided with the blue and green zones for the lower pressure flames and with the yellow luminous carbon zone for the higher pressure flames, and that the photographs taken with the 8700-Å filter coincided with the white or yellow luminous zone at all pressures. To determine the nature of the flame emission at these separate wavelengths, an emission spectrum of the flame was taken with a 0.25-m monochromator in the spectral regions of 3100 Å and 8700 Å at both 1 and 50 atm. At 1 atm, the OH rotational band structure was clearly visible in the vicinity of 3100 Å, whereas at 8700 Å, only the continuum from carbon-particle emission was evident. At 50 atm, the carbon-particle continuum at 8700 Å was still observed; but the OH band structure was no longer evident near 3100 Å, there being only a faint continuum of increasing intensity with increasing wavelength, undoubtedly due to carbon-particle emission. The lack of OH band structure could be due either to a very low OH concentration in the flame at 50 atm, or to excited OH falling to the ground state by collision damping rather than by emission. On the basis of these separate spectral studies it was concluded that the color photographs in figure 7 did indeed give a fair representation of the significant reaction zones, including both the OH region and the luminous carbon zone, and, further, that it was unlikely that zones of significant gas-phase reactions were missed, even for the higher pressure flames where carbon-particle luminosity becomes so intense.

To obtain estimates of the methane reaction volumes, the reaction zones shown in the color photographs were traced on fine-grid graph paper, and the areas so defined were analytically revolved about the center line of the flame. In estimating such reaction volumes, possible image distortion, caused by refraction of light by density gradients in the flame, was ignored. A plot of the resulting reaction volumes as a function of pressure is shown in figure 16 along with their estimated error bounds.

If the reaction volumes given in figure 16 are divided into the known (constant) flow rate for methane of 41.8 sccm expressed in moles/sec, the average overall methane consumption rate $\bar{r}^{E}_{CH_4}$ is obtained. This rate is plotted as a function of pressure in figure 17. As limiting cases for methane consumption, the average overall rates of consumption of methane based on gas-phase reaction kinetics $\bar{r}^{stoich}_{CH_4}$ and based on carbon-particle oxidation kinetics $\bar{r}^{carbon}_{CH_4}$ were calculated as described subsequently and are also plotted in figure 17 for comparison.

In calculating the limiting reaction rate for gas-phase methane oxidation $\bar{r}^{stoich}_{CH_4}$, the following assumptions are made. All methane is consumed by

reaction with oxygen, and the concentration of oxygen in the presence of methane during reaction is just that needed for complete combustion, that is, the stoichiometric amount. For this stoichiometric combustion, the mole fractions of methane x_{CH_4} and of oxygen x_{O_2} are taken to be 0.095 and 0.190, respectively, the same amounts that would exist in a premixed stoichiometric methane-air flame. The kinetic expression used for calculating the overall rate of methane consumption (i.e., the single-step conversion of CH_4 and O_2 to CO_2 and H_2O) is

$$r_{CH_4} = 10^{14} e^{-32500/RT} C_{CH_4} C_{O_2} \tag{5}$$

which is based on a study of methane-air diffusion flames by Tuteja (ref. 25). Because the temperature in equation (5) represents an average temperature throughout the reaction zone, which is somewhat uncertain but obviously smaller than the measured peak flame temperature T_f, several average temperatures less than T_f were employed. These were arbitrarily taken to be 50 K, 100 K, and 150 K below T_f, and the kinetic reaction rate $\bar{r}^{stoich}_{CH_4}$ plotted in figure 17 has been calculated for these three average temperatures. There are only minor differences in the predicted kinetic reaction rates for the three temperatures. The fact that all these kinetic rates are more than 2 orders of magnitude greater than the experimental average reaction rate $\bar{r}^{E}_{CH_4}$ indicates that the experimental reaction rate is strongly diffusion controlled at all pressures, as expected.

Since at high pressure, methane consumption proceeds to a large extent through (solid) carbon intermediates, a reaction rate $\bar{r}^{carbon}_{CH_4}$ has also been calculated. This reaction rate is based on the assumptions that all methane is instantaneously and completely pyrolyzed to carbon particles and hydrogen, and that oxidation of these carbon particles is the rate-controlling step. To estimate this oxidation rate of carbon particles, the expression of Nagle and Strickland-Constable for the oxidation rate of pyrolytic graphite was used in accordance with the suggestion of Appleton (ref. 29) that it fairly accurately describes the oxidation rate of carbon particles within a flame. For this reaction, as before, the stoichiometric amount of oxygen was assumed to be in the reaction vicinity of the carbon particles (and hydrogen). Since the reaction-rate expression of Nagle and Strickland-Constable (as given by Appleton (ref. 29) and reproduced in appendix E) is per unit area of carbon surface, the size of the carbon particles in the flame affects the overall reaction rate. Calculations were made for spherical particles, both 50 Å and 100 Å in diameter, sizes which are within the bounds observed by Narasimhan and Foster (ref. 16) in their study of carbon-particle growth in turbulent methane-air flames. For simplicity, the calculation of $\bar{r}^{carbon}_{CH_4}$ was made at only one average temperature, $T_{av} = T_f - 100$ K. The resulting reaction rate is plotted in figure 17. Although the kinetic prediction for $\bar{r}^{carbon}_{CH_4}$ is

below that for $\bar{r}^{stoich}_{CH_4}$, it is still more than an order of magnitude greater than $\bar{r}^{E}_{CH_4}$. Therefore, regardless of the reaction path for the consumption of methane, the reaction rate in the present diffusion flame appears to be definitely limited by diffusion.

The average rate of formation of nitrogen oxides $\bar{r}^{E}_{NO_X}$ in the flame was calculated from the plot of $\bar{r}^{E}_{CH_4}$ in figure 17, the plot of I_m in figure 13, and equation (4). A plot of $\bar{r}^{E}_{NO_X}$ as a function of pressure is shown in figure 18. This estimate of the average rate of formation of NO_X in the flame can now be compared with formation rates predicted by the conventional two-step Zeldovich mechanism for NO formation:

$$O + N_2 \underset{k_r}{\overset{k_f}{\rightleftarrows}} NO + N \tag{6}$$

$$N + O_2 \underset{k_r}{\overset{k_f}{\rightleftarrows}} NO + O \tag{7}$$

The generally accepted values for the reaction-rate constants, given by Bracco (ref. 30), are

$$k_{f6} = 1.36 \times 10^{14}\ e^{-75400/RT}$$

$$k_{r6} = 3.1 \times 10^{13}\ e^{-334/RT}$$

$$k_{f7} = 6.4 \times 10^{9}\ Te^{-6250/RT}$$

$$k_{r7} = 1.5 \times 10^{9}\ Te^{-38640/RT}$$

If elementary rate expressions, based on equations (6) and (7), are written for the rate of formation of NO (dC_{NO}/dt), the usual steady-state assumption for nitrogen atoms is made, and an order of magnitude analysis is used to eliminate negligible terms, the customary expression for the rate of formation of NO is obtained:

$$r_{NO} = \frac{dC_{NO}}{dt} = 2k_{f6}C_O C_{N_2} \tag{8}$$

One approach which has been used in the literature in applying equation (8) has been to assume that oxygen atoms are in equilibrium with oxygen molecules:

$$O_2 + M \underset{k_r}{\overset{k_f}{\rightleftarrows}} 2O + M \tag{9}$$

where the equilibrium constant K_O given by Bracco is

$$K_O = \frac{C_O^2}{C_{O_2}} = \frac{k_{f9}}{k_{r9}} = 3.54 \times 10^4 \frac{1}{T} e^{-118000/RT} \tag{10}$$

Substitution of equation (10) into equation (8) permits the calculation of the predicted reaction rate, r_{NO}, provided that C_{O_2} and C_{N_2} are known. Unfortunately, unlike the situation for a premixed flame, there is some uncertainty regarding the proper values for these concentrations in a diffusion flame. For nitrogen, species concentration profiles in fuel-air diffusion flames reported by Tuteja (ref. 25) and Takagi and coworkers (ref. 28) show a large concentration of nitrogen, virtually the same as in air, extending well into the combustion zone. Hence, to a very good approximation, the mole fraction of nitrogen in the region of important NO formation may be taken to be 0.79. The proper concentration to use for oxygen is considerably more uncertain. Obviously, the maximum concentration of oxygen that can exist is a mole fraction of 0.21; this value, therefore, represents an upper limit. A lower limit for oxygen mole fraction can be obtained by replacing r_{CH_4} in equation (5) with $\bar{r}^E_{CH_4}$ from figure 17 and solving for that $\bar{C}_{O_2}$ which would give the observed methane reaction rate at stoichiometric concentrations of methane and oxygen in the flame zone. This was done for $T_{av} = T_f - 100$ K, and the values of $\bar{C}_{O_2}$ obtained are plotted in figure 19 as average mole fraction $\bar{x}_{O_2}$ as a function of pressure. These values of $\bar{x}_{O_2}$ are considered a lower limit of oxygen mole fraction for NO formation because they represent the average mole fraction of oxygen in the combustion zone, whereas maximum NO formation is known to occur slightly to the air side of the combustion zone where temperature is highest and oxygen concentration is somewhat greater than in the fuel combustion zone. To get an intermediate, more realistic value for oxygen mole fraction which may actually exist in the NO formation zone of a diffusion flame (at least at 1 atm), species profiles reported by Tuteja (ref. 25) and Takagi and coworkers (ref. 28) in 1-atm diffusion flames can be used. Profiles reported in both references indicate that the mole fraction of NO in the flame has virtually the same shape as the temperature profile, which peaks slightly to the air side of the combustion zone. (A qualitative sketch of a typical profile is depicted in fig. 20.) Since NO seems to be formed in the highest temperature zone in the flame, a number of species profiles from references 25 and 28 for the mole fraction of oxygen were integrated over that region of the

flame within about 300 K of the peak in the temperature profile.[6] This gave an approximate average oxygen mole fraction of about 0.04.

The three values for $\bar{x}_{O_2}$ presented in the preceding paragraph were used in equations (8) and (10) to predict $\bar{r}_{NO_X}$. Such predictions are plotted in figure 18 for one average temperature, $T_{av} = T_f - 100$ K. Certainly the most striking aspect of these predicted rates in figure 18 is that they are as much as 2 orders of magnitude smaller than the experimentally observed rate. To dispel the possible argument that $T_{av} = T_f - 100$ K is really too low, similar rate predictions were made for $\bar{x}_{O_2} = 0.21$ and 0.04 for T_f, the peak temperature observed in the flame. These rates are also plotted in figure 18, and they, too, fall well below the experimentally observed rate. The predicted rates are only weakly dependent on pressure because the decreasing flame temperature is sufficient to cancel any increase in rate caused by increasing pressure. The slight increase in the predicted rates between 20 atm and 50 atm is due largely to the increase in pressure, since flame temperatures between 20 atm and 50 atm differ by only 50 K. In strong contrast to the shape of the predicted rate curves is the shape of the experimental rate curve, which increases markedly with pressure at low pressures but begins to level off at higher pressures.

Experimental rates of NO_X formation considerably higher than rates predicted by the Zeldovich mechanism, assuming oxygen-atom equilibrium, have often been observed and have been the subject of much discussion in the literature. The discrepancy is generally attributed to the presence of superequilibrium concentrations of oxygen atoms in the flame; that is, during the combustion process, oxygen atoms are formed as reaction intermediates in concentrations greater than those which would exist if the oxygen atoms were in chemical equilibrium with oxygen molecules in the flame. (See, for instance, refs. 27, 31, 32, 33, and 34 for premixed flames and ref. 28 for diffusion flames.) Since the Zeldovich mechanism is still accepted as the proper reaction mechanism, at least for lean and near-stoichiometric flames, the problem then becomes one of experimentally determining what the true mole fraction of oxygen atoms really is. Customarily the mole fraction of oxygen atoms is determined either from a detailed kinetic combustion mechanism or by calculating that oxygen-atom mole fraction required to give the experimentally observed rate of NO_X formation. For this purpose, the rate expression in equation (8) based on the Zeldovich mechanism is usually used, and results are usually expressed as ratios of superequilibrium concentration to the equilibrium concentration of oxygen atoms. Such calculations have been made for the present data for $T_{av} = T_f - 100$ K, and the results are plotted in figure 21 as the ratio $x_{O,req'd}/x_{O,eq}^{stoich}$. The mole fraction $x_{O,req'd}$ is that oxygen-atom mole

---

[6] The value of 300 K was chosen for the following reason. If equation (10) is substituted into equation (8) and an average reaction temperature on the order of 2000 K is assumed, the rate of NO formation drops by 2 orders of magnitude for a 300-K temperature decrease. Hence, all significant NO formation must occur within at least 300 K of the peak temperature.

fraction required by equation (8) to give the observed experimental rate of formation $\bar{r}^{E}_{NO_X}$ for $\bar{x}_{N_2} = 0.79$ and $T_{av} = T_f - 100$ K, and $x^{stoich}_{O,eq}$ is the equilibrium oxygen-atom mole fraction for stoichiometric premixed combustion at the same temperature T_{av} calculated with the computer program of Svehla and McBride (ref. 35).

From figure 21, the required oxygen-atom ratio is about 30 at 1 atm, increases to a maximum value of about 10 000 near 35 atm, and thereafter decreases slightly. The value of 30 at 1 atm is in the neighborhood of typical theoretical and experimental values reported for premixed flames at $\phi = 1$. (See table I.) Hence, the present data are not inconsistent with other results in the literature at 1 atm. But as pressure increases, the required oxygen-atom ratio increases to very large values. The only known study reporting the effect of pressure on required oxygen-atom ratio is that of Ay and Sichel (ref. 34), who theoretically calculated required oxygen-atom ratios for methane-air flames at $\phi = 0.6$. These ratios increase from about 100 at 1 atm to only about 180 at 30 atm. This increase by a factor of about 2 is considerably less than the factor of over 300 observed in the present study, but the calculations of Ay and Sichel (ref. 34) are for a much lower value of ϕ (0.6) than that assumed to be effective for diffusion flames (1.0). It must also be appreciated that a diffusion flame differs considerably from a premixed flame, because even though it may be reasonable to assume an overall average equivalence ratio of unity throughout the combustion zone, in actual fact the local equivalence ratio decreases from very large values on the fuel side to virtually zero on the air side of the flame zone. (See fig. 20.) Table I shows that for isothermal combustion (refs. 31 and 33) the required oxygen-atom ratio increases with increasing equivalance ratio, but for adiabatic combustion (ref. 34) the required oxygen-atom ratio is a minimum at $\phi = 1$. The predictions of Ay and Sichel (ref. 34) for adiabatic combustion are believed to be more appropriate to the situation which exists across the flame zone in a diffusion flame, since for adiabatic combustion the peak temperature is reached near $\phi = 1$ and decreases for both larger and smaller values of ϕ, a situation roughly approximating that for local values of ϕ throughout the flame zone in a diffusion flame. Thus, because for a diffusion flame the required oxygen-atom ratio is really an integrated average across the flame front, and because according to the calculations of Ay and Sichel, the ratio is a minimum for a local ϕ of unity, the required oxygen-atom ratio would be expected to be somewhat larger than that for a premixed flame at $\phi = 1$. The present value of required oxygen-atom ratio of 30 at 1 atm (fig. 21), being somewhat larger than the theoretically calculated value of Ay and Sichel (ref. 34) of 20, is at least in the right direction.

At higher pressures the present values of required oxygen-atom ratio increase rapidly (fig. 21), a situation which is consistent with NO being formed in an increasingly fuel-rich environment as pressure increases. For instance, table I shows that for rich flames the required oxygen-atom ratio can reach values well into the thousands. This possible situation of NO being formed in an increasingly fuel-rich environment as the pressure increases can readily be rationalized in a diffusion flame. Many authors (refs. 27, 31, 33, and 34) accept the concept of oxygen-atom superequilibrium as a satisfactory

explanation for NO formation rates in lean and near-stoichiometric flames; however, for rich flames a number of authors (see, for instance, refs. 33, 36, 37, 38, and 39) reason that additional mechanisms involving nitrogen reactions with hydrocarbons or hydrocarbon fragments are necessary to explain observed NO formation rates. In a diffusion flame, there is an abundance of nitrogen well into the fuel side of the combustion zone to permit such reactions to occur (see fig. 20), and at higher pressures the rates of these reactions should be enhanced. Furthermore, the reaction zone thins as pressure increases, and the average mole fraction of oxygen molecules in the flame zone begins to decrease (see fig. 19), and along with it, possibly, the oxygen-atom concentration. Hence, it seems reasonable that an increasing fraction of the total NO formed could be formed by hydrocarbon-nitrogen reactions as pressure is increased, particularly at the lower temperatures which accompany the increase in pressure (lower temperatures favor reduced oxygen-atom concentrations).

Takagi and coworkers (ref. 28) reached a similar conclusion in their study of turbulent hydrogen-air and propane-air diffusion flames at 1 atm, in which the temperatures were reduced by varying amounts of nitrogen dilution. Although they could satisfactorily explain their results for hydrogen flames by appealing to an oxygen-atom overshoot, for the propane-air flames they would have had to postulate unreasonably high oxygen-atom overshoots to account for their results in the reduced temperature flames. Accordingly, in agreement with a number of other authors, they reasoned that for premixed flames reactions involving nitrogen with hydrocarbons or hydrocarbon fragments must be occurring. It may be of some additional interest to note that for the 1-atm turbulent propane-air diffusion flame of reference 28 issuing from a 2-mm-diameter fuel port, an overall average NO formation rate of 8.4 ppm/msec was obtained. This compares with an average rate of about 12.0 ppm/msec for the present laminar methane-air diffusion flame at 1 atm issuing from a 3.06-mm-diameter fuel port. (These low values for hydrocarbon fuels can be contrasted with the much higher value of 67 ppm/msec reported in reference 28 for hydrogen-air flames with the same burner system.)

Discussion of Molar Emission Index Curve

Unfortunately, none of the foregoing discussion explains the maximum in the molar emission index as a function of pressure shown in figure 13. Although several explanations for this phenomenon are possible, the present data do not permit a clear choice among them at this time. One of the more likely explanations is the possibility that at higher pressures the NO concentration in the flame has essentially reached its equilibrium value, which decreases as pressure is increased. The computer program of Svehla and McBride (ref. 35) was used to calculate equilibrium mole fractions of NO for stoichiometric methane-air combustion at various assumed average flame temperatures; these mole fractions were then divided by the stoichiometric mole fraction of methane to obtain an equilibrium molar emission index (which is the same as that which would exist for a premixed flame). These values of $I_{m,eq}$ are plotted in figure 22 in comparison with the I_m data from the present study. At low pressures, $I_{m,eq}$ is far above the experimental I_m and it is safe to say that the equilibrium NO concentration has not been reached. However, $I_{m,eq}$

decreases rapidly with increasing pressure (recall that there is also an associated decrease in temperature), and at higher pressures, $I_{m,eq}$ tends to follow the decrease in experimentally measured I_m. The implication from this comparison is that at low pressures the increase in experimental I_m is due to an actual increase in the rate of NO formation as pressure increases, whereas at higher pressures the observed decrease is due to the fact that the equilibrium concentration of NO, which decreases with increasing pressure, has been reached in the flame. (The temperature effect here is small, because above 20 atm, T_f, and therefore T_{av}, decreases by only 50 K.)

Although this explanation is appealing, it cannot be accepted uncritically. The concept of stoichiometric combustion in the flame zone of a diffusion flame is only a reasonable overall approximation; and treatment of this zone as if it were effectively premixed, and making equilibrium calculations on this basis, is an obvious oversimplification of the true situation. The absolute magnitude of average temperatures T_{av} has little fundamental significance because of the uncertain temperature distribution in the reaction zone. Hence, it would be inappropriate to conclude from figure 22 that the most reasonable value for T_{av} is close to T_f - 50 K. However, the qualitative picture suggested by figure 22 is, nevertheless, somewhat compelling; at high pressures, a decrease in I_m seems to be caused by equilibrium concentrations of NO having been attained. This proposition could be investigated experimentally by studying flames of CO and H_2 and making similar equilibrium calculations. The temperatures of flames of these fuels should change very little with pressure because no solid carbon is formed to radiate heat from the flame as is the case with hydrocarbon flames. It would also be interesting to study NO formation near an electrically heated carbon surface undergoing air oxidation, and to vary the temperature of the surface as well as the total pressure. This would permit a detailed examination of temperature effects independent of pressure effects. Flames of premixed fuel and air could also offer useful information because no assumptions would have to be made regarding the equivalence ratio of such flames. However, premixed flames are considerably more hazardous to work with at high pressures than diffusion flames because of potential problems of flashback and detonation.

Another phenomenon possibly occurring in the present methane-air flame could account for a maximum in the I_m curve, but to get any information about it is extremely difficult. As pressure changes, the concentrations of oxygen molecules and atoms in the zone where most of the NO is formed may also change, and in an uncertain way. Figure 19 shows the average oxygen concentration in the flame zone required to give agreement between the experimentally observed methane reaction rate and an overall kinetic expression for methane oxidation assuming stoichiometric combustion. This figure indicates that the oxygen mole fraction may decrease by a factor of about 4.5 from 1 atm to 50 atm. However, the oxygen concentration in the zone where most of the NO is formed is uncertain. If the temperature gradient on the air side of the flame zone becomes steeper as pressure is increased (as a result of a thinner reaction zone), the high-temperature zone, necessary for substantial NO formation, will move closer into the combustion zone where the concentration of oxygen is lower, and the rate of NO formation will decrease. However, as discussed previously, more NO may be formed through nitrogen-hydrocarbon reactions. Experimentally, both

concentration and temperature profiles are difficult to measure in the present system because of the poor accessibility of the flame for probing and also because of the difficulties in making spatially resolved measurements in such small flames with such thin reaction zones. Furthermore, the presence of large concentrations of carbon in the flame makes effective probe sampling additionally difficult. If some experimental means could be devised by which the flame could be experimentally probed for both composition and temperature, the results would be extremely valuable in interpreting the NO_x data for the present methane-air flame, as well as for flames of other fuels. One potentially attractive alternate solution for gaining information regarding composition and temperature profiles would be to formulate a detailed analytical model of the flame, accounting for both reaction kinetics and mass transport as a function of pressure. However, one severely limiting aspect to such an approach is the lack of suitable kinetic mechanisms for the formation, growth, and combustion of carbon particles within the flame. If such a detailed analytical model of the flame could be successfully formulated, however, it could provide much insight into many of the unexplained phenomena occurring in the present diffusion flame.

A third factor which might be partially responsible for the maximum in the I_m curve as a function of pressure is that significant amounts of (solid) carbon are formed in the flame at increased pressures. Figure 11 shows that the number of carbon particles in the flame may increase by as much as 5 or 6 orders of magnitude as pressure is increased from 1 atm to 10 atm and that there is still some further increase above 10 atm. The presence of these carbon particles in the flame, though not altering the final composition of the effluent from the flame (i.e., CO_2 and H_2O), indicates that the elementary reactions governing combustion at high pressure (when carbon is formed) are different from those at low pressure (when carbon is virtually absent). It has already been proposed that nonequilibrium concentrations of oxygen atoms in the flame are responsible for determining the rate of NO formation (at least in lean and near-stoichiometric flames). All that would be required for a reduction in NO formation rate would be a reduction in this nonequilibrium oxygen-atom concentration caused by a change in reaction mechanism. For instance, if fewer oxygen atoms were produced by intermediate reactions during the oxidation of carbon in the flame than during the homogeneous oxidation of gaseous methane, the formation of NO in the flame would tend to be retarded, and at a sufficiently high carbon concentration, a decrease in the molar emission index would occur as carbon concentration in the flame increased further. The presence of solid carbon in the flame could possibly reduce NO formation in another way. As an increasing number of carbon particles are formed in the flame at higher pressures, a rapidly increasing amount of carbon is tied up in these particles, with substantially less carbon present as hydrocarbon fragments and radicals. (An estimate of the number of carbon atoms in a carbon particle can be obtained from eq. (E3). From the two terms in the denominator on the right side of eq. (E3), it is calculated that only one carbon particle, 100 Å in diameter, ties up more than 50 000 carbon atoms.) Hence, if direct nitrogen attack on hydrocarbon radicals in the flame is an important intermediate step in the formation of NO, NO formation should be reduced when substantial amounts of carbon are formed in the flame, simply because the concentration of these hydrocarbon radicals is reduced.

Unfortunately, known kinetic mechanisms for the oxidation of methane (see, for instance, refs. 31 and 34), which predict the occurrence of superequilibrium concentrations of oxygen atoms in the flame, do not account for the formation, growth, and subsequent combustion of carbon in the flame. Hence, it does not appear to be currently possible to examine theoretically the effect of solid carbon in a methane flame on oxygen-atom superequilibrium concentration or hydrocarbon radical concentration. However, several experiments can be proposed which could provide some information on this effect. Some of these experiments are identical with those already proposed for investigating the possibility that a decrease in I_m is caused by equilibrium concentrations of NO having been reached. One such experiment would be to measure the molar emission index for CO and H_2 flames. Since carbon is not formed in either of these flames, the absence or presence of a maximum in the molar emission index would tend to support or refute the proposal of a carbon effect. Although existing data already indicate that the molar emission index of CO flames does not attain a maximum as a function of pressure (see data from ref. 23 in fig. 14), these data need verification because air was not used as the oxidizer, the opposed-jet burner geometry employed was markedly different from the present geometry, and complete burning was not always attained. As an additional, but experimentally difficult step, the CO and H_2 flames could be seeded with finely divided carbon particles to investigate their effect. Flames of hydrocarbons which produce carbon more readily than methane, such as ethylene, ethane, and propane, could also be investigated. With these flames, any effects due to carbon should be observed at lower pressures, although these flames very likely will smoke more readily. Premixed stoichiometric flames of methane and air do not form carbon at 1 atm, and none is expected even at high pressures. Hence, such flames could also be used to investigate the effect of carbon on NO formation. To study NO formation associated with combustion of carbon particles in a flame, a solid carbon body could be electrically heated in a stream of air. Significant NO formation would occur only in the region of high temperature immediately adjacent to the surface, the temperature of which could be both measured and controlled quite accurately.

In the present study of NO formation, fuel and air flow rates have been held constant, and it has been assumed that molar emission index is relatively insensitive to them. With air in considerable excess, all the air that can possibly diffuse to the flame is available, and hence, the effect of air flow should be minimal. Since molar emission index is normalized by fuel consumption, its dependence on fuel flow rate should also be minimal. As long as the flame remains laminar, total combined flow rate is likewise expected to have only a small effect on molar emission index. However, in future studies, all these factors should be considered, and the sensitivity of molar emission index (and of temperature) to the various fuel, air, and combined flow rates should be experimentally determined.

CONCLUDING REMARKS

A high-pressure flame system has been designed and constructed for studying nitrogen oxide formation in fuel-air combustion. Its advantages and limitations have been demonstrated by tests with a confined laminar methane-air

diffusion flame over the pressure range from 1 to 50 atm. In all tests (except those in which stability limits were determined), methane and air flow rates were held constant at 41.8 standard cm^3/min (sccm) and 2450 sccm, respectively. The methane issued coaxially from a 3.06-mm-diameter port into a coflowing stream of air contained within a 20.5-mm-diameter chimney.

A number of interesting phenomena have been observed in the behavior of this methane-air diffusion flame over the pressure range from 1 to 50 atm. Measurements of nitrogen oxide concentrations in the combustion products of this flame have been made, and these, too, reveal many interesting phenomena. On the basis of the present experimental data, analyses of these data, and comparisons with other experimental and theoretical results, the following observations and conclusions are offered:

(1) The shape of the methane-air diffusion flame changes from a wide convex flame at 1 atm to a slender concave flame at 50 atm. The most notable change in shape occurs below about 5 atm.

(2) Accompanying the change in the shape of the flames is a marked increase in carbon in the flame, and hence, the luminosity of the flame, as the pressure is increased from 1 to 50 atm. It is conjectured that this increasing amount of carbon in the flame is largely responsible for its change in shape. Accordingly, any mathematical description of the diffusional combustion of methane with air at pressures even moderately above 1 atm must properly account for the formation and subsequent combustion of carbon in the flame.

(3) Although the height of the flame changes to some extent with pressure, this change is not large, and with the exception of 50-atm flames, the flames were typically on the order of 10 mm high.

(4) As total pressure of the flame is increased, the limits of stability and extinction are greatly reduced, and the limits within which the flame smokes are greatly increased. The most pronounced changes occur between 1 and 5 atm. Regardless of flow rate, all flames at 50 atm were found to be luminous. Even at only 20 atm, a nonluminous flame could be produced only in a very limited region of low fuel and air flow rates.

(5) Concentrations of nitrogen oxides produced during combustion were measured and reported as a molar emission index, that is, the moles of nitrogen oxides formed per mole of methane consumed. The molar emission index, which is 0.85×10^{-3} at 1 atm, increases rapidly as pressure is increased; it reaches a maximum value of 1.21×10^{-3} at about 9 atm; and thereafter it decreases slowly until at 50 atm it is back to the same value that it was at 1 atm. This maximum occurs in spite of the fact that the peak temperature in the flame decreases from about 2130 K at 1 atm to about 1850 K at 20 atm, and thereafter, decreases relatively little as pressure increases. It is particularly significant that for gas turbine engine applications, at all pressures above 1 atm and approaching 50 atm, the molar emission index is greater than that at 1 atm.

(6) Similar data for emission index for gas turbine engines, over a more limited range of pressures than that of the present study, also reach a maximum with pressure.

(7) For the methane-air diffusion flame, overall average methane reaction rates were estimated from the data and compared with limiting kinetic predictions. This comparison shows that the predicted reaction rates are more than an order of magnitude greater than the experimental rates and therefore confirms that the combustion is diffusion controlled at all pressures.

(8) Overall average nitrogen oxide formation rates were also calculated from the data. These rates are far greater than nitric oxide formation rates predicted by the conventional two-step Zeldovich mechanism with oxygen atoms assumed to be in equilibrium with oxygen molecules.

(9) The concentrations of oxygen atoms required to give the observed nitrogen oxide formation rates were calculated according to the Zeldovich mechanism and then divided by the equilibrium oxygen-atom concentration to obtain required superequilibrium oxygen-atom ratios. At 1 atm the value of this ratio, 30, is close to literature values for premixed flames, but increases well into the thousands above 5 atm, reaching 10 000 at 35 atm. At these higher pressures, it may be that an increasing amount of nitric oxide is formed through nitrogen-hydrocarbon reactions in addition to the Zeldovich mechanism.

(10) The maximum observed in the curve of molar emission index as a function of pressure could be due to several possible causes:

(a) At low pressures the molar emission index is determined by the kinetic rate of formation of nitric oxide; hence, it increases with pressure because of the effect of increasing pressure on reaction rate. But at high pressures the equilibrium concentration of NO may be reached, and since this equilibrium concentration decreases with increasing pressure, the molar emission index also decreases.

(b) The concentrations of oxygen molecules and oxygen atoms in the zone where most of the nitric oxide is formed may be changing with pressure in such a way as to produce a maximum value for molar emission index.

(c) The increasing amount of carbon formed in the flame as pressure increases may alter the combustion mechanism to produce fewer oxygen atoms or fewer hydrocarbon radicals. At sufficiently high pressures, this decreasing concentration of oxygen atoms or hydrocarbon radicals would cause a decrease in nitric oxide formation.

(11) The present preliminary data do not permit a definite choice among the above alternatives for explaining the observed maximum in molar emission index. Accordingly, a number of experiments which would aid in making such a choice have been suggested.

Langley Research Center
National Aeronautics and Space Administration
Hampton, VA 23665
March 1, 1977

APPENDIX A

DEPENDENCE OF PSEUDOEQUIVALENCE RATIO ON VOLUMETRIC FLOW RATE OF FUEL AND AIR AT STANDARD CONDITIONS

Define

$$S = \left(\frac{\dot{n}_{fuel}}{\dot{n}_{air}}\right)_{stoich} \tag{A1}$$

Thus, for methane, S = 0.105. The pseudoequivalence ratio based on actual molar flow rates to the burner is defined as

$$\phi' = \frac{1}{S}\frac{\dot{n}_{fuel}}{\dot{n}_{air}} = \frac{1}{S}\frac{(p\dot{V}/RT)_{fuel}}{(p\dot{V}/RT)_{air}} \tag{A2}$$

But at standard conditions,

$$\frac{p\dot{V}}{RT} = \frac{(1)\dot{V}_{STP}}{R(293)} \tag{A3}$$

where $\dot{V}_{STP}$ is the volumetric flow rate at standard conditions (1 atm, 293 K). Therefore,

$$\phi' = \frac{1}{S}\frac{\dot{V}_{STP,fuel}}{\dot{V}_{STP,air}} \tag{A4}$$

APPENDIX B

DILUTION CALCULATIONS

The combustion of methane in air for ϕ' less than 1 can be expressed as

$$CH_4 + \frac{2}{0.21\phi'}(0.21O_2 + 0.79N_2) = CO_2 + 2H_2O + \left(\frac{2}{\phi'} - 2\right)O_2 + \frac{2}{\phi'}\left(\frac{0.79}{0.21}\right)N_2 \qquad (B1)$$

and the mole fraction of water vapor produced then becomes

$$x_{H_2O} = \frac{2}{1 + 2 + \left(\frac{2}{\phi'} - 2\right) + \frac{2}{\phi'}\left(\frac{0.79}{0.21}\right)} \qquad (B2)$$

For the usual conditions of operation in the present report ($\phi' = 0.162$), $x_{H_2O} = 0.033$, which is greater than the saturation value at 1 atm and room temperature of 296 K, about $x_{H_2O} = 0.028$. At a temperature of 288 K (arbitrarily about 8 K below room temperature), the partial pressure of water vapor is 0.0167 atm, which corresponds to a mole fraction of 0.0167 at a total pressure of 1 atm. Thus, to prevent condensation in unheated sample lines, the mole fraction of water vapor must be less than or equal to 0.0167. This low mole fraction can be attained by nitrogen dilution, where

$$x_{H_2O} = \frac{2}{1 + 2 + \left(\frac{2}{\phi'} - 2\right) + \frac{2}{\phi'}\left(\frac{0.79}{0.21}\right) + n_{N_2,dil}} \qquad (B3)$$

where $n_{N_2,dil}$ is the number of moles of nitrogen added for dilution per mole of methane consumed.

In the present study, the molar ratio of nitrogen to total reactants or combustion products customarily was 2.4, which, from equation (B3) with $\phi' = 0.162$, gives $x_{H_2O} = 0.0098$. This value corresponds to a saturation temperature of 279.9 K at 1 atm and 354 K at 50 atm. Therefore, the use of unheated sample lines at 1 atm and sample lines at elevated pressures heated to 393 K is adequate to prevent condensation.

APPENDIX C

GAS CHROMATOGRAPHIC SYSTEM

The gas chromatographic system employed in the early checkout tests consisted of two separate gas chromatographs in series as shown in figure 23. The first chromatograph has two 3.658-m × 0.3175-cm-diameter columns of 100 × 120 mesh Porapak Q, and the second has two 1.829-m × 0.635-cm-diameter Molecular Sieve 5A columns. Carrier gas (helium) sweeps the sample through the sample loop and onto the Porapak Q column in the first gas chromatograph where the light gases (H_2, O_2, N_2, CO, and CH_4) come through early with only minimal separation. These gases are carried to the second gas chromatograph where they are separated and analyzed on the Molecular Sieve 5A column. Just before CO_2, H_2O and compounds with longer retention times are eluted from the Porapak Q column in the first chromatograph, the switching valve (SV, fig. 23) is thrown, and directs them to vent. This procedure permits analysis for the compounds with longer retention times on the Porapak Q column in the first gas chromatograph but prevents contamination of the Molecular Sieve 5A column in the second. Pressure imbalance during switching is minimized by the regulating valves (RV in fig. 23) which have been preset to provide flow restrictions equal to those of the molecular sieve columns. The CO_2, H_2O, and compounds with longer retention times are analyzed by thermal conductivity as they are eluted from the Porapak Q column, with the exception of hydrocarbons, which are analyzed with flame ionization. Fixed capillary restriction coils provide the proper splitting of the flows to the thermal conductivity and flame ionization detectors.

Operating conditions for the two chromatographs are as follows:

	Chromatographs	
	Porapak Q	Molecular Sieve 5A
Temperature, K, of -		
Column oven	Programed[a]	358
Thermal conductivity cell	473	383
Injection port	473	398
Transfer zone	473	383
Bridge current, mA	150	200
Helium carrier flow rate, sccm	41	41
Flame ionization detector:		
Flame temperature, K	473	---
Hydrogen fuel flow rate, sccm	25	---
Air flow rate, sccm	500	---

[a]The oven temperature is programed to be isothermal at 353 K for 3 min following injection, then to increase 15 K/min up to 453 K and to hold at 453 K for 6 min before recycling.

APPENDIX C

Switching of the effluent from the first gas chromatograph to vent to prevent this effluent from being directed to the second gas chromatograph is accomplished at 1.75 to 1.80 min after sample injection. A 0.5-cm^3 sample loop provides a sufficiently large sample for a good analysis without introducing too large a pressure pulse upon injection. An even larger sample loop could be used satisfactorily if desired.

APPENDIX D

ESTIMATE OF CARBON CONCENTRATION IN THE FLAME

An estimate of the mass concentration of carbon in the tip of the flame can be obtained from the brightness temperature measurements in the tip of the flame and the calculated temperature of the flame. By using equation (2) in the text and by approximating the exponential by the first two terms of a Taylor series expansion, the spectral emissivity of the carbon particles in the flame can be approximated by

$$\varepsilon_\lambda \approx K_\lambda c L \tag{D1}$$

The spectral extinction coefficient K_λ is given by Mie theory (see, for instance, ref. 40) as

$$K_\lambda = \frac{36\pi}{\rho_C} \frac{F(\lambda)}{\lambda} \tag{D2}$$

where ρ_C is the density of a carbon particle, λ is the wavelength, and

$$F(\lambda) = \frac{n^2\kappa}{\left[n^2(1 - \kappa^2) + 2\right]^2 + 4n^4\kappa^2} \tag{D3}$$

and where n and κ are the refractive and absorption indices in the complex index of refraction $m = n - in\kappa$. Equations (D1) and (D2) can be combined and solved for c, the mass concentration of carbon, to get

$$c = \frac{\rho_C \lambda \varepsilon_\lambda}{36\pi\ F(\lambda)\ L} \tag{D4}$$

This expression can be evaluated at $\lambda = 6500$ Å (650 nm) by taking $n = 1.57$, $\kappa = 0.28$ (see ref. 41 for propane soot), and $\rho_C = 2.0$ g/cm^3 (a virtual constant for most carbon or soot particles) to obtain

$$c = 3.38 \times 10^{-5} \frac{\varepsilon_\lambda}{L} \tag{D5}$$

To evaluate c, then, an estimate of the spectral emissivity ε_λ is needed. This estimate can be obtained from the definition of spectral emissivity,

$$E_\lambda(T_f)\ \varepsilon_\lambda = E_\lambda(T_{b,\lambda}) \tag{D6}$$

where T_f is the flame temperature, $T_{b,\lambda}$ is the brightness temperature at wavelength λ, and $E_\lambda(T)$, the Planck function at temperature T, is given by

$$E_\lambda(T) = \frac{c_1 \lambda^{-5}}{e^{c_2/\lambda T} - 1} \tag{D7}$$

Neglecting the 1 in the denominator (valid for $\lambda T \leq 0.3$) and substituting into equation (D6) yields

$$\varepsilon_\lambda = e^{\frac{c_2}{\lambda}\left(\frac{1}{T_f} - \frac{1}{T_{b,\lambda}}\right)} \tag{D8}$$

Values for c are obtained by substituting the brightness temperature data at 6500 Å and the calculated flame temperature into equation (D8) and by inserting the resulting values of ε_λ into equation (D5) along with values for L obtained from the flame photographs in figure 7. These values of c are shown as a function of pressure in figure 10. Since the required temperature data are not available below 5 atm, the portion of the curve in figure 10 from 5 atm down to 2.5 atm was constructed by a reasonable extrapolation of the brightness temperature data toward zero at 1 atm and extrapolation of the flame temperature data towards 2130 K at 1 atm (100 K below the adiabatic flame temperature of 2230 K to account for heat loss by molecular radiation). If spherical carbon particles are assumed, the number density of carbon particles N_C in the flame is related, by definition, to the mass concentration of carbon in the flame by

$$c = N_C\left(\frac{\pi {d_C}^3}{6}\right)\rho_C \tag{D9}$$

Hence,

$$N_C = \frac{6c}{\pi \rho_C {d_C}^3} = 0.9549\,\frac{c}{{d_C}^3} \tag{D10}$$

and N_C can be estimated from equations (D5) and (D10) provided that information on the size of the carbon particles is available.

APPENDIX E

REACTION-RATE EXPRESSION FOR OXIDATION OF SOLID CARBON

According to reference 29, a suitable expression for the specific oxidation rate of solid carbon within a flame is given by the equation (attributed to Nagle and Strickland-Constable):

$$w = \chi\left(\frac{k_A p x_{O_2}}{1 + k_Z p x_{O_2}}\right) + k_B p x_{O_2}(1 - \chi) \tag{E1}$$

where w is in moles/cm^2-sec and

$$\chi = \frac{1}{1 + \dfrac{k_T}{k_B p x_{O_2}}}$$

$$k_A = 20e^{-30000/RT}$$

$$k_B = 4.46 \times 10^{-3}\ e^{-15200/RT}$$

$$k_T = 1.51 \times 10^{5}\ e^{-97000/RT}$$

$$k_Z = 21.3e^{4100/RT}$$

To express the specific surface reaction rate w given in equation (E1) as a reaction rate per unit volume in the flame, w must be multiplied by a factor expressing the total surface area of the carbon particles in the flame per unit volume of the reaction zone in the flame. For spherical particles, this factor is

$$\Gamma = \pi d_C^{\,2} N_C \tag{E2}$$

where d_C is the particle diameter and N_C is the number density of particles in the flame. For the limiting case when all the carbon atoms in the methane fuel appear in the flame as carbon particles,

$$(N_C)_{max} = N^{o}_{CH_4} \Bigg/ \left(\frac{\pi d_C^{\,3}}{6}\right)\left(\frac{\rho_C N_A}{M_C}\right) \tag{E3}$$

where $(N_C)_{max}$ is the number density of carbon particles in the flame zone if all carbon appears as soot particles; the first term in the denominator on the right side is the volume of a carbon particle of diameter d_C; the second term in the denominator is the number of carbon atoms per unit volume of a carbon particle, where ρ_C is the density of a carbon particle (2.00 g/cm^3), M_C is the molecular weight of carbon, and N_A is Avogadro's number; and $N^o_{CH_4}$ is the number of carbon atoms available in the methane fuel per unit volume of the reaction zone in the flame assuming stoichiometric combustion in the flame zone. Expressing $N^o_{CH_4}$ in terms of mole fraction yields

$$N^o_{CH_4} = \frac{x^o_{CH_4} p N_A}{RT} \tag{E4}$$

where $x^o_{CH_4}$ is the mole fraction of methane fuel that would exist in the flame zone under stoichiometric conditions if none had been converted to soot. Substituting equations (E3) and (E4) into (E2) and taking $x^o_{CH_4} = 0.095$ results in

$$\Gamma_{max} = 0.0417 \frac{p}{d_C T} \tag{E5}$$

This expression is the maximum possible total surface area of carbon particles of diameter d_C in the flame per unit volume of the reaction zone in the flame.

REFERENCES

1. Burke, S. P.; and Schumann, T. E. W.: Diffusion Flames. Proceedings of the First Symposium on Combustion and the Second Symposium on Combustion, Combustion Inst., c.1965, pp. 2-11.

2. Barr, John: Diffusion Flames. Fourth Symposium (International) on Combustion, Williams & Wilkins Co., 1953, pp. 765-771.

3. Maahs, Howard G.: Interference of Oxygen, Carbon Dioxide, and Water Vapor on the Analysis for Oxides of Nitrogen by Chemiluminescence. NASA TM X-3229, 1975.

4. Weinberg, F. J.: Optics of Flames Including Methods for the Study of Refractive Index Fields in Combustion and Aerodynamics. Butterworth & Co. (Publ.) Ltd., 1963.

5. Kuhn, G.; and Tankin, R. S.: Spectroscopic Measurements To Determine Temperature and Carbon Particle Size in an Absorbing Propane Diffusion Flame. J. Quant. Spectros. & Radiat. Transfer, vol. 8, no. 6, June 1968, pp. 1281-1292.

6. Ribaud, G.; Laure, Y.; and Gaudry, H.: The Measurement of Flame Temperatures. J. Inst. Fuel, vol. 12, no. 64, Mar. 1939, pp. S18-S30.

7. McAdams, William H.: Heat Transmission. Third ed., McGraw-Hill Book Co., Inc., 1954.

8. D'Alessio, A.; Di Lorenzo, A.; Beretta, F.; and Venitozzi, C.: Optical and Chemical Investigations on Fuel-Rich Methane-Oxygen Premixed Flames at Atmospheric Pressure. Fourteenth Symposium (International) on Combustion, Combustion Inst., 1973, pp. 941-953.

9. Gaydon, A. G.; and Wolfhard, H. G.: Flames. Their Structure, Radiation, and Temperature. Third ed., Rev. Chapman and Hall Ltd. (London), 1970.

10. Jost, Wilhelm (Huber O. Croft, transl.): Explosion and Combustion Processes in Gases. McGraw-Hill Book Co., Inc., 1946.

11. Barr, J.: Combustion in Vitiated Atmospheres. II - Some Preliminary Studies of Diffusion Flames. Fuel, vol. XXVIII, no. 9, Sept. 1949, pp. 200-205.

12. Barr, J.; and Mullins, B. P.: Concerning Combustion in Vitiated Atmospheres. Rep. No. R.44, Natl. Gas Turbine Establ., Min. Supply (British), June 1949.

13. Parker, W. G.; and Wolfhard, H. G.: Carbon Formation in Flames. J. Chem. Soc., 1950, pp. 2038-2049.

14. Powell, H. N.: The Height of Diffusion Flames and the Relative Importance of Mixing and Reaction Rates. Fifth Symposium (International) on Combustion, Reinhold Pub. Corp., 1955, pp. 290-302.

15. McArragher, J. S.; and Tan, K. J.: Soot Formation at High Pressures: A Literature Review. Combust. Sci. & Technol., vol. 5, no. 5, July 1972, pp. 257-261.

16. Narasimhan, K. S.; and Foster, P. J.: The Rate of Growth of Soot in Turbulent Flow With Combustion Products and Methane. Tenth Symposium (International) on Combustion, Combustion Inst., 1965, pp. 253-257.

17. Powell, H. N.; and Browne, W. G.: Some Fluid Dynamic Aspects of Laminar Diffusion Flames. Sixth Symposium (International) on Combustion, Reinhold Pub. Corp., c.1957, pp. 918-922.

18. Benson, R.; Samuelsen, G. S.; and Peck, R. E.: Oxides of Nitrogen Transformation While Sampling Combustion Products Containing Carbon Monoxide. [Paper] WSS/CI 76-11, Combustion Inst., Apr. 1976.

19. Diehl, Larry A.; and Holdeman, James D.: Gaseous Exhaust Emissions From a JT8D-109 Turbofan Engine at Simulated Cruise Flight Conditions. NASA TM X-3290, 1975.

20. Norgren, Carl T.; and Ingebo, Robert D.: Effect of Fuel Vapor Concentrations on Combustor Emissions and Performance. NASA TM X-2800, 1973.

21. Quigg, H. T.: Reduction of Pollutants From Aircraft Turbine by Fuel Selection and Prevaporization. Res. & Dev. Rep. 6607-73 (Contract N00140-72-C-6969), Phillips Pet. Co., Oct. 1973. (Available from DDC as AD 769 099.)

22. Sullivan, D. A.; and Mas, P. A.: A Critical Review of NO_x Correlations for Gas Turbine Combustors. Paper No. 75-WA/GT-7, American Assoc. Mech. Eng., Nov.-Dec. 1975.

23. Newitt, Dudley M.; and Lamont, Frank G.: Gaseous Combustion at High Pressures, Part XVI: - Nitric Oxide Formation in Continuous High-Pressure Flames of Carbonic Oxide in Oxygen-Nitrogen Atmospheres. Proc. Roy. Soc. London, Ser. A, vol. CXXXIX, no. A 837, Jan. 2, 1933, pp. 83-93.

24. Perry, John H., ed.: Chemical Engineers' Handbook. Third ed., McGraw-Hill Book Co., Inc., 1950.

25. Tuteja, Arjun Dev: The Formation of Nitric Oxide in Diffusion Flames. Ph. D. Thesis, Univ. of Wisconsin, 1972.

26. Fristrom, R. M.; and Westenberg, A. A.: Flame Structure. McGraw-Hill Book Co., c.1965.

27. Sarofim, A. F.; and Pohl, J. H.: Kinetics of Nitric Oxide Formation in Premixed Laminar Flames. Fourteenth Symposium (International) on Combustion, Combustion Inst., 1973, pp. 739-754.

28. Takagi, Toshimi; Ogasawara, Mitsunobu; Fujii, Kenichi; and Daizo, Masahito: A Study on Nitric Oxide Formation in Turbulent Diffusion Flames. Fifteenth Symposium (International) on Combustion, Combustion Inst., 1974, pp. 1051-1059.

29. Appleton, John P.: Soot Oxidation Kinetics at Combustion Temperatures. Atmospheric Pollution by Aircraft Engines, AGARD-CP-125, Sept. 1973, pp. 20-1 - 20-11.

30. Bracco, Frediano V.: Nitric Oxide Formation in Droplet Diffusion Flames. Fourteenth Symposium (International) on Combustion, Combustion Inst., 1973, pp. 831-842.

31. Bowman, Craig T.: Kinetics of Nitric Oxide Formation in Combustion Processes. Fourteenth Symposium (International) on Combustion, Combustion Inst., 1973, pp. 729-738.

32. Thompson, D.; Brown, T. D.; and Beér, J. M.: Formation of NO in a Methane-Air Flame. Fourteenth Symposium (International) on Combustion, Combustion Inst., 1973, pp. 787-799.

33. Iverach, D.; Basden, K. S.; and Kirov, N. Y.: Formation of Nitric Oxide in Fuel-Lean and Fuel-Rich Flames. Fourteenth Symposium (International) on Combustion, Combustion Inst., 1973, pp. 767-775.

34. Ay, J. H.; and Sichel, M.: Theoretical Analysis of NO Formation Near the Primary Reaction Zone in Methane Combustion. Combust. & Flame, vol. 26, no. 1, Feb. 1976, pp. 1-15.

35. Svehla, Roger A.; and McBride, Bonnie J.: FORTRAN IV Computer Program for Calculation of Thermodynamic and Transport Properties of Complex Chemical Systems. NASA TN D-7056, 1973.

36. Fenimore, C. P.: Formation of Nitric Oxide in Premixed Hydrocarbon Flames. Thirteenth Symposium (International) on Combustion, Combustion Inst., 1971, pp. 373-380.

37. Just, T.: Grundlagen der Schadstoffemission. Paper 29, Deutsche Gesellschaft fur Luft und Raumfahrt, Jahrestagung, 7th (Kiel, West Germany), Sept. 1974.

38. Eberius, K. H.; and Just, Th.: NO Formation in Fuel Rich Flames: A Study of the Influence of the Hydrocarbon Structure. Atmospheric Pollution by Aircraft Engines, AGARD-CP-125, Sept. 1973, pp. 16-1 - 16-8.

39. Jachimowski, Casimir J.: Analytical Study of Mechanisms for Nitric Oxide Formation During Combustion of Methane in a Jet-Stirred Combustor. NASA TN D-8098, 1975.

40. Van de Hulst, H. C.: Light Scattering by Small Particles. John Wiley & Sons, Inc., c.1957.

41. Dalzell, W. H.; and Sarofim, A. F.: Optical Constants of Soot and Their Application to Heat-Flux Calculations. Trans. ASME, Ser. C: J. Heat Transfer, vol. 91, Feb. 1969, pp. 100-104.

TABLE I.- REQUIRED OXYGEN-ATOM RATIOS FOR PREMIXED FLAMES

Author	Method	System	p, atm	T, K	ϕ	$x_{O,req'd}/x_{O,eq}$
Bowman (ref. 31)	Theoretical calculation	CH_4-O_2-N_2	1 ↓	2200 ↓	0.8 1.0 1.4	30 80 250
Ay and Sichel (ref. 34)[a]	Theoretical calculation	CH_4-O_2-N_2	1 ↓ 30	Adiabatic ↓	0.6 .8 1.0 1.4 .6	100 35 20 1000 180
Thompson, Brown, and Beér (ref. 32)	Experimental	CH_4-air	1 1	1800 to 2000 1800 to 2000	0.75 .96	12 4
Iverach, Basden, and Kirov (ref. 33)	Experimental	Ethylene-air	1 ↓	2045 ↓	0.8 1.0 1.4 1.55	7 20 1100 5500

[a]Values of required oxygen-atom ratio attributed to Ay and Sichel were obtained from cross plots of figures published by them.

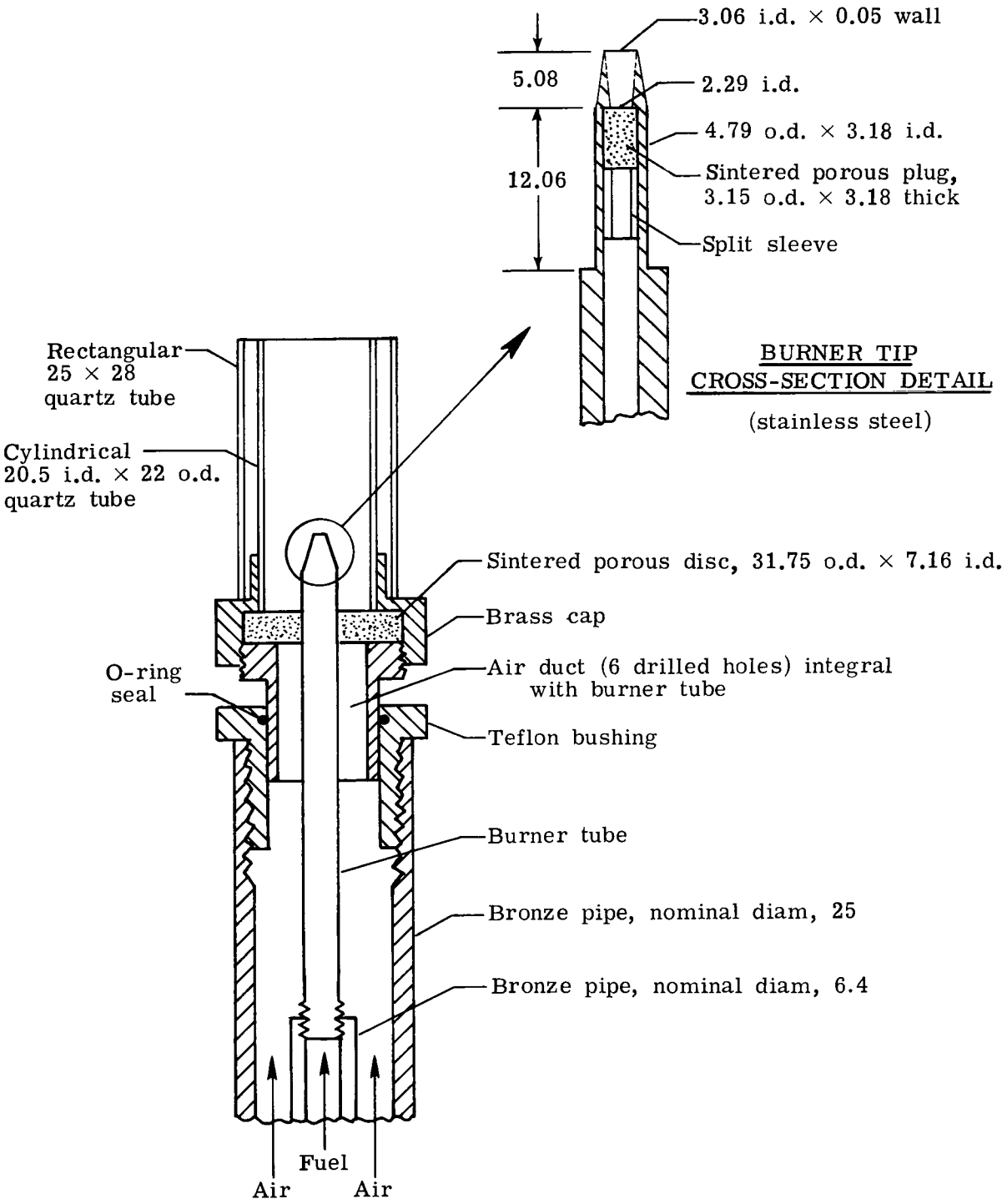

Figure 1.- Burner assembly and detail. All dimensions are in millimeters.

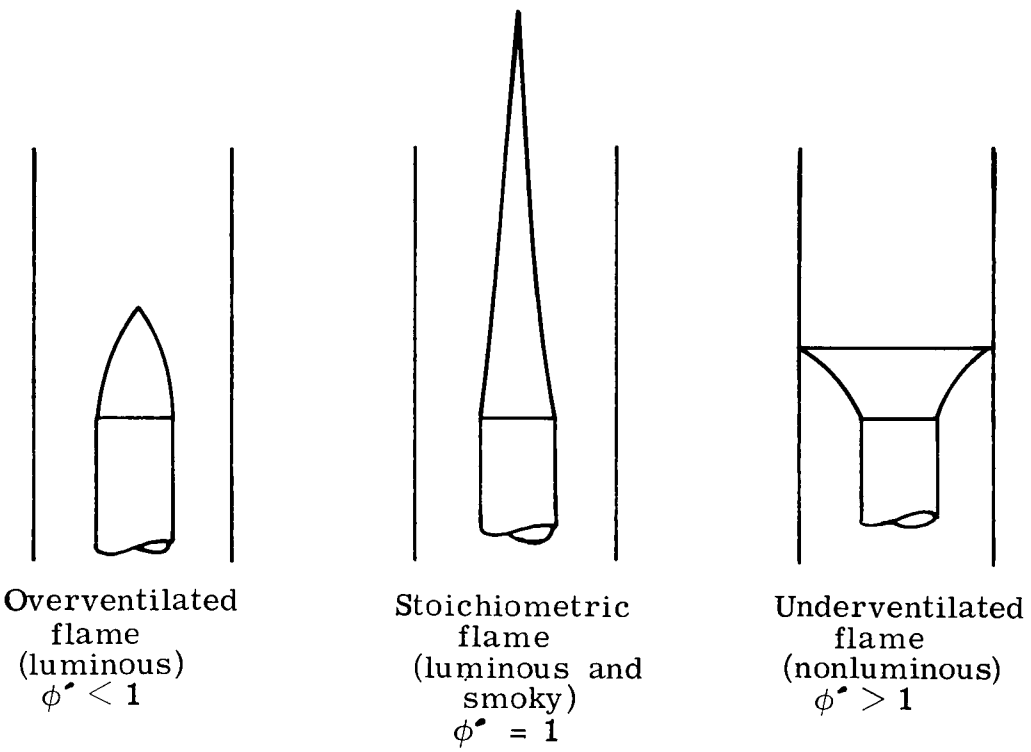

Figure 2.- Types of Burke and Schumann diffusion flames.

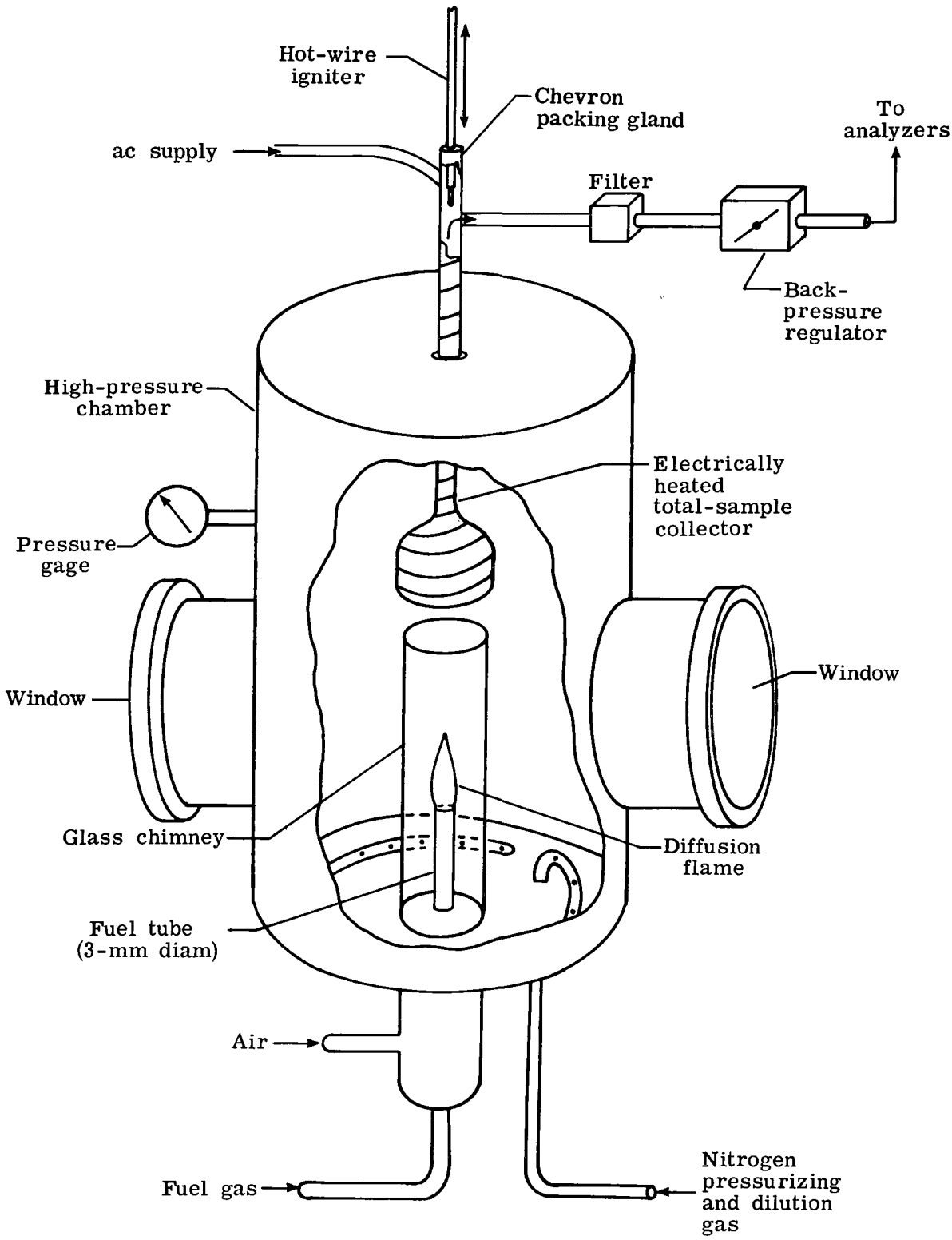

Figure 3.- Schematic diagram of burner and sample collection system.

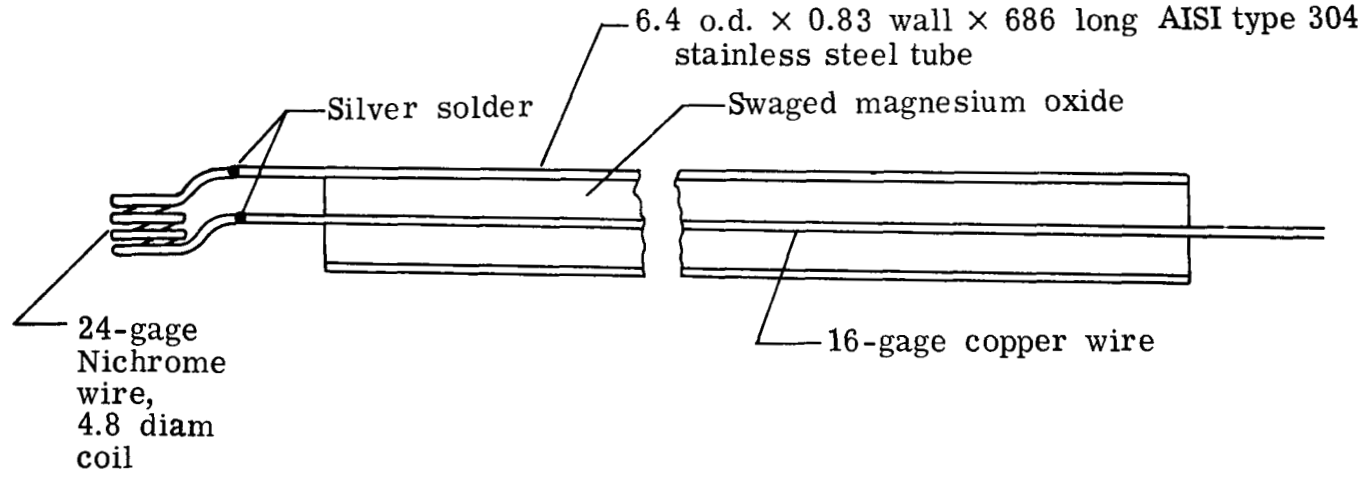

Figure 4.- Hot-wire igniter probe. Dimensions are in millimeters.

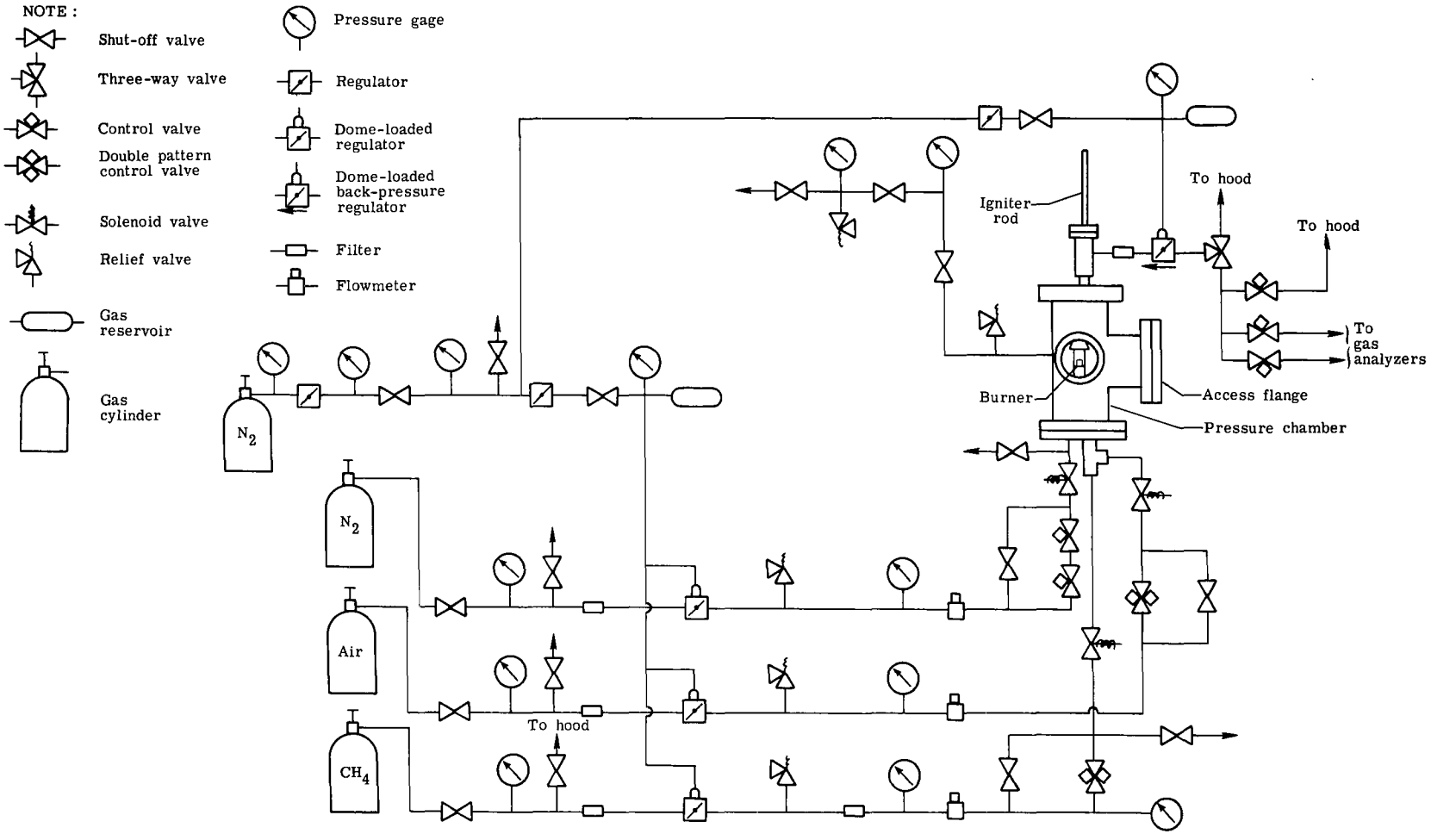

Figure 5.- Schematic of flow and pressure control system.

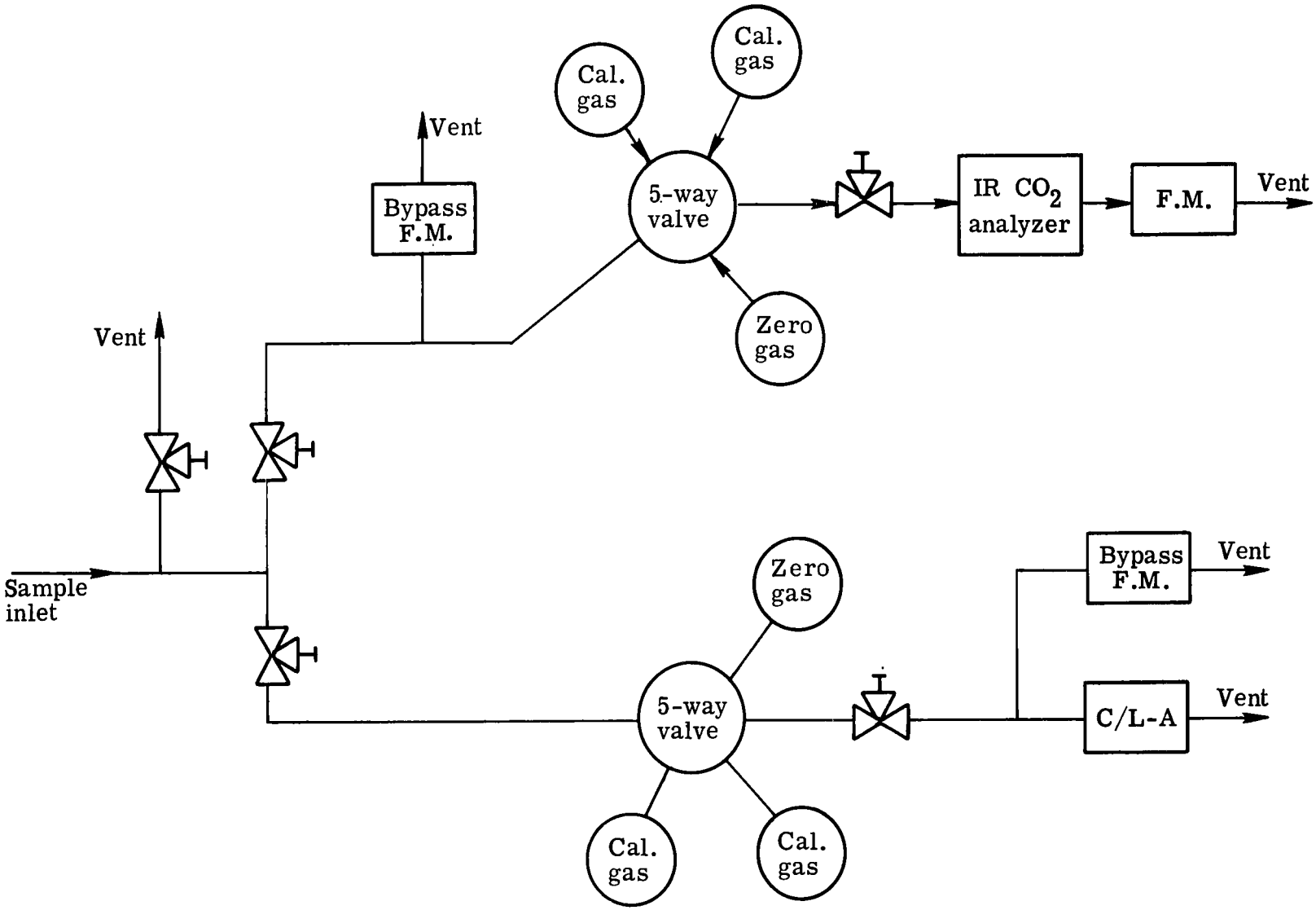

Figure 6.- Diagram of gas analysis system.

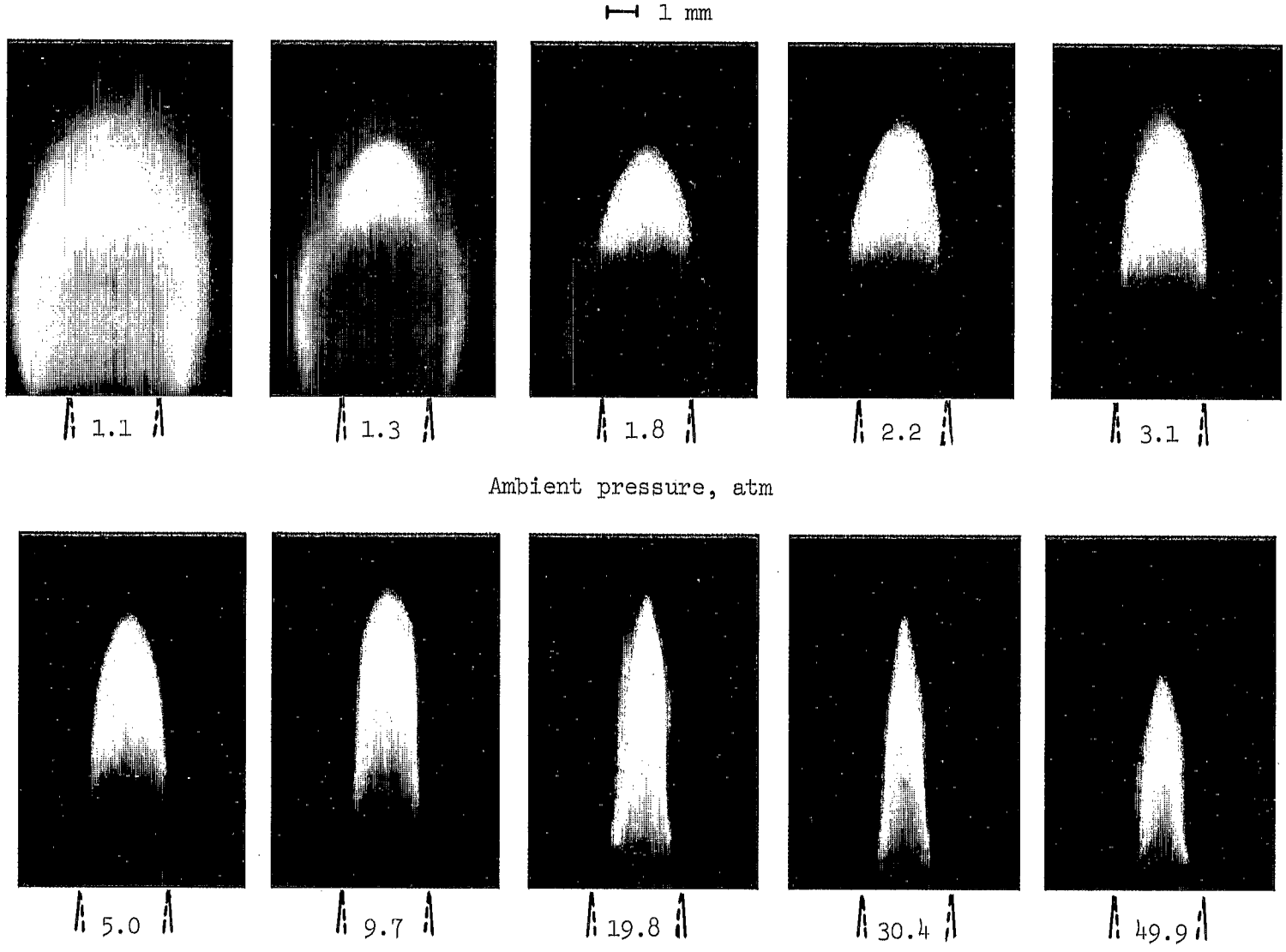

Figure 7.- Photographs of methane-air diffusion flames for various ambient pressures. Methane flow rate, 41.8 sccm; air flow rate, 2450 sccm; burner diameter, 3.06 mm.

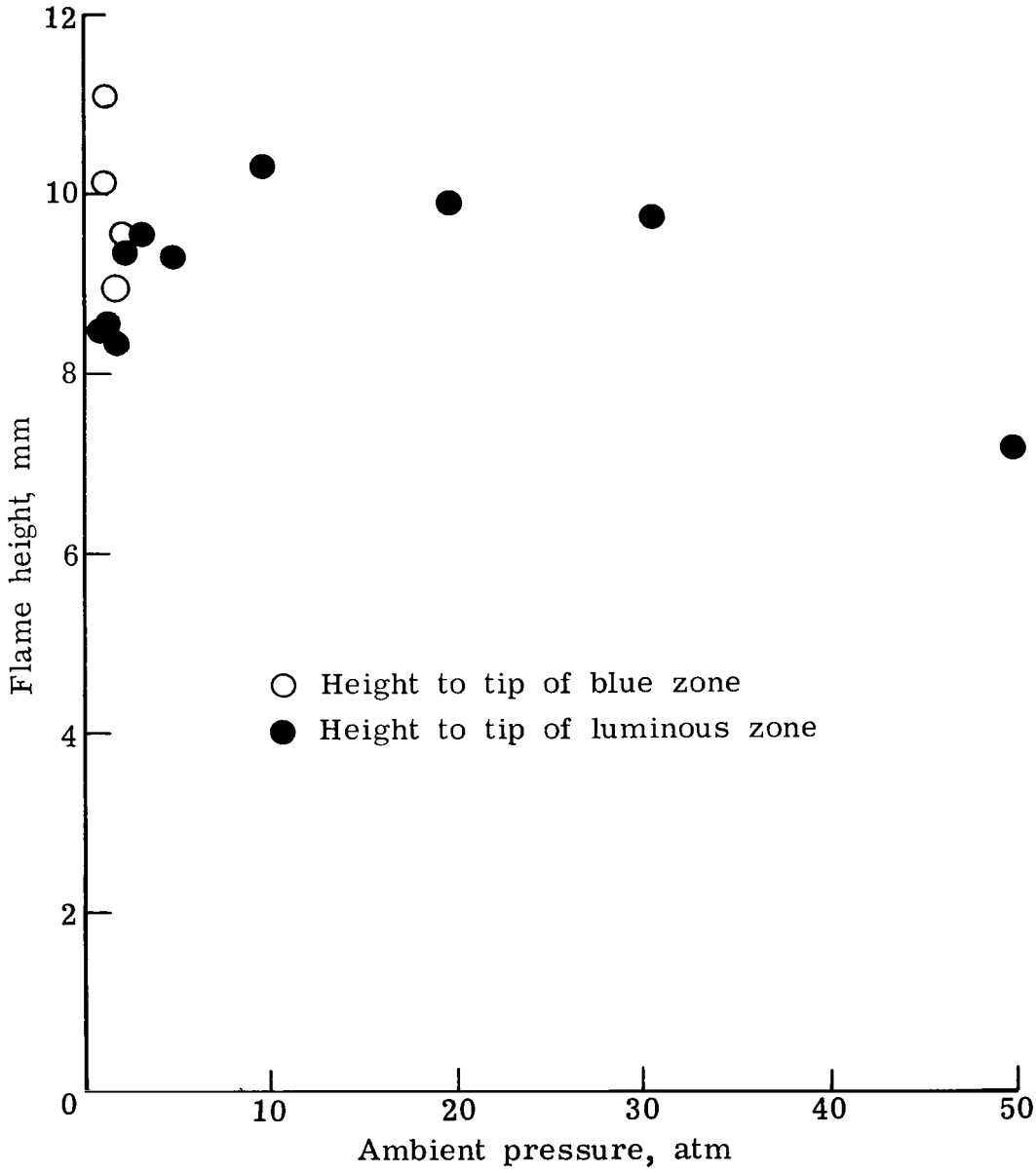

Figure 8.- Flame height as function of pressure.

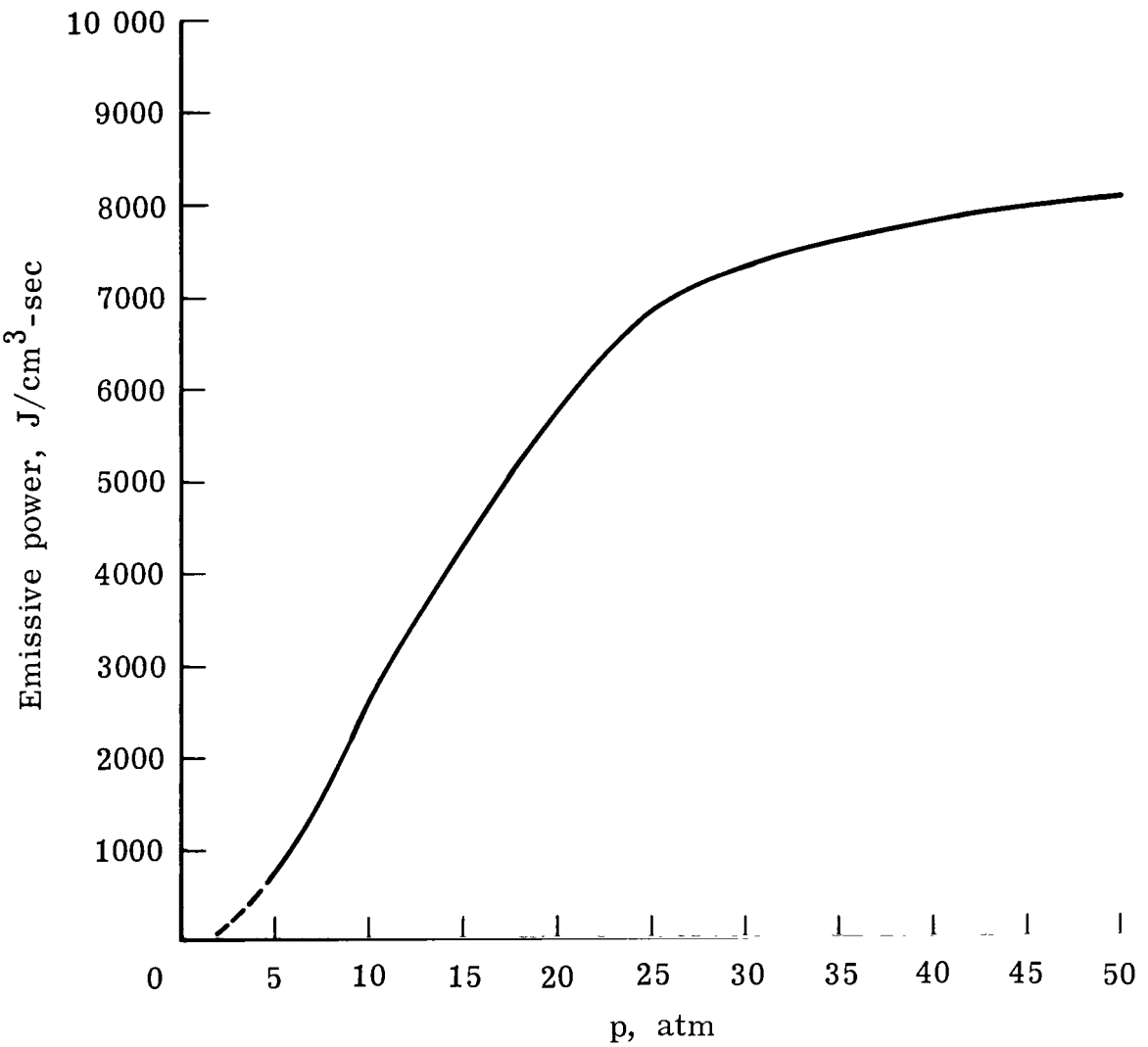

Figure 9.- Monochromatic emissive power at 6500 Å as function of pressure.

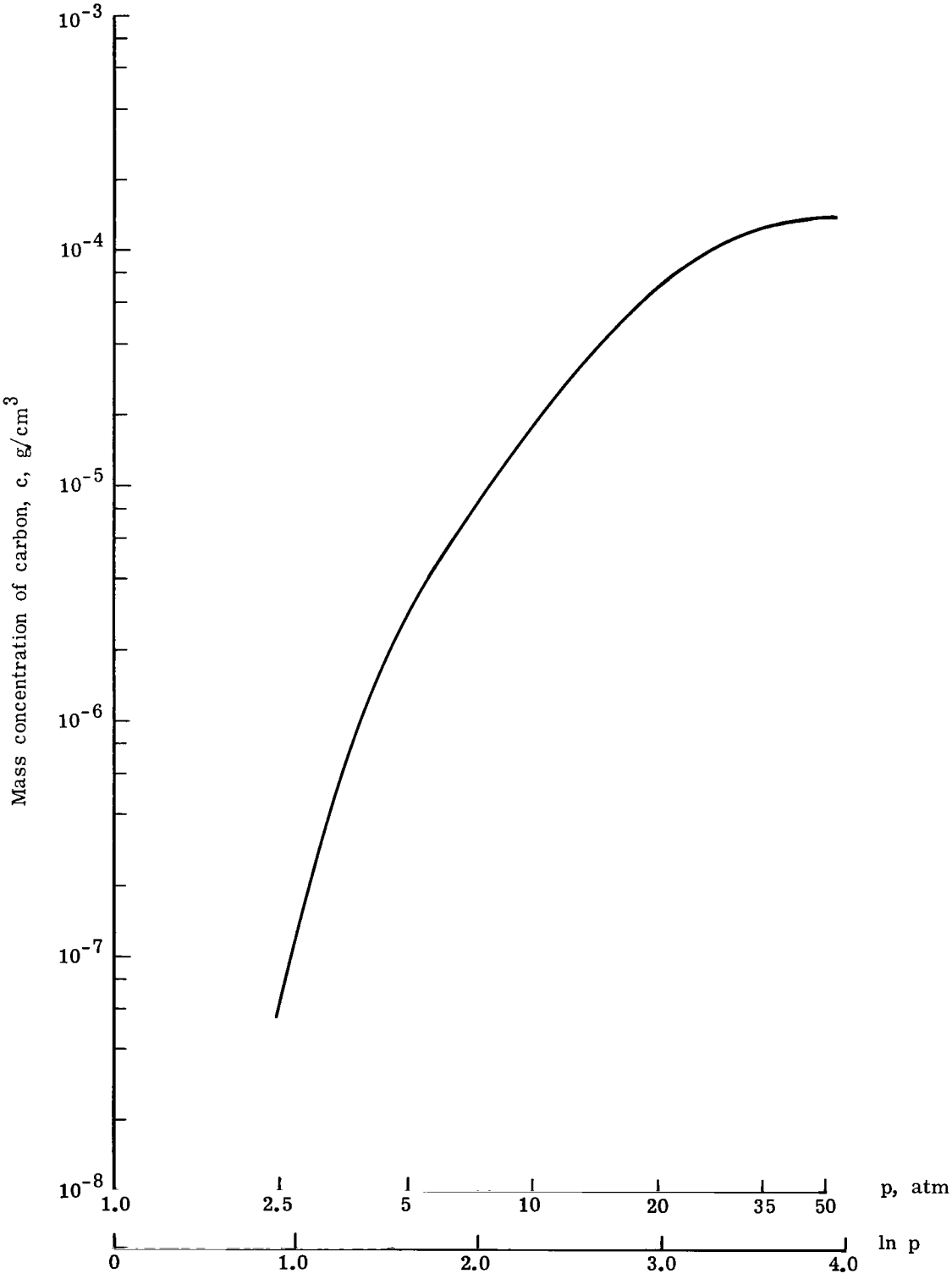

Figure 10.- Mass concentration of carbon as function of pressure.

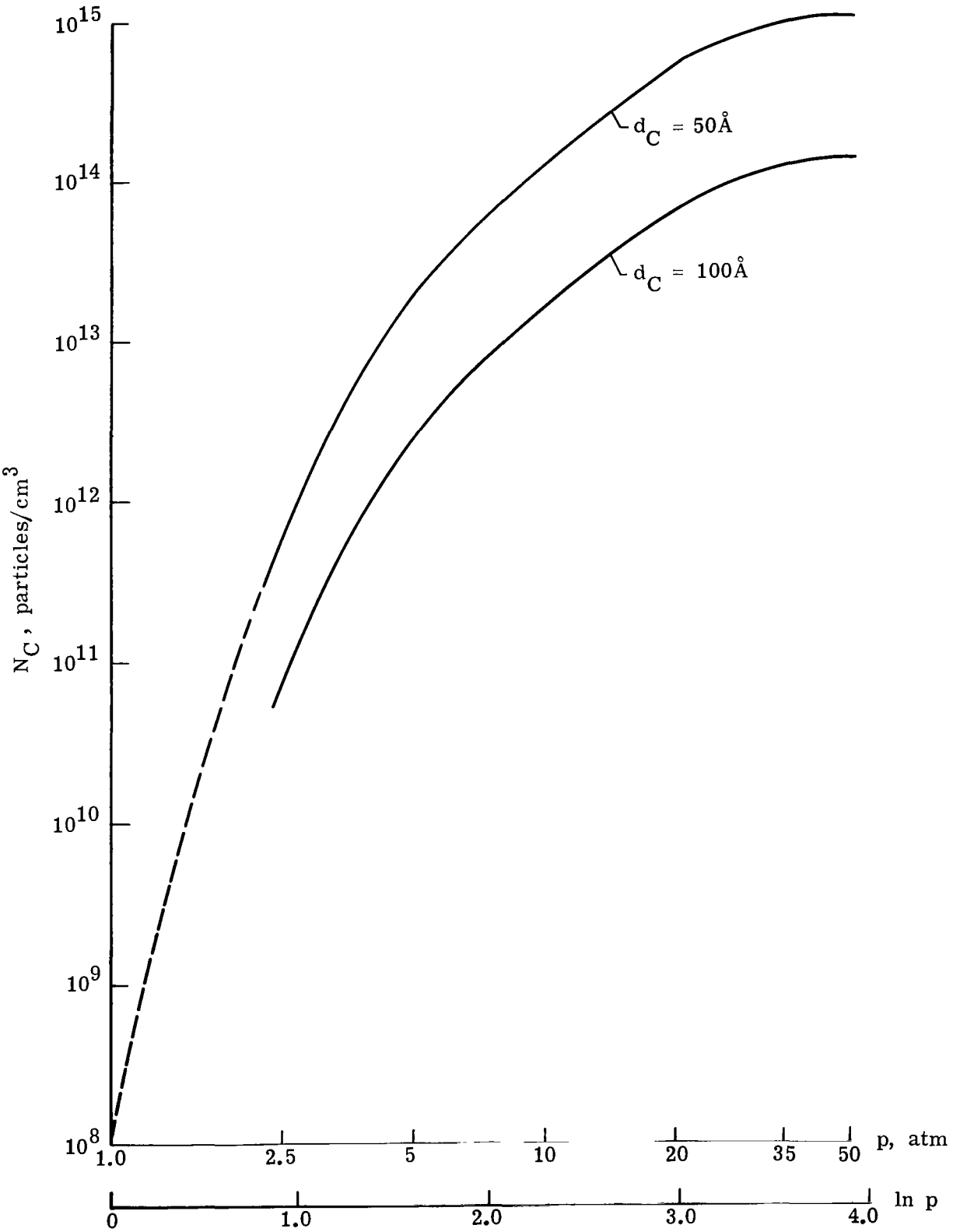

Figure 11.- Carbon-particle density as function of pressure. Dashed curve indicates extrapolation.

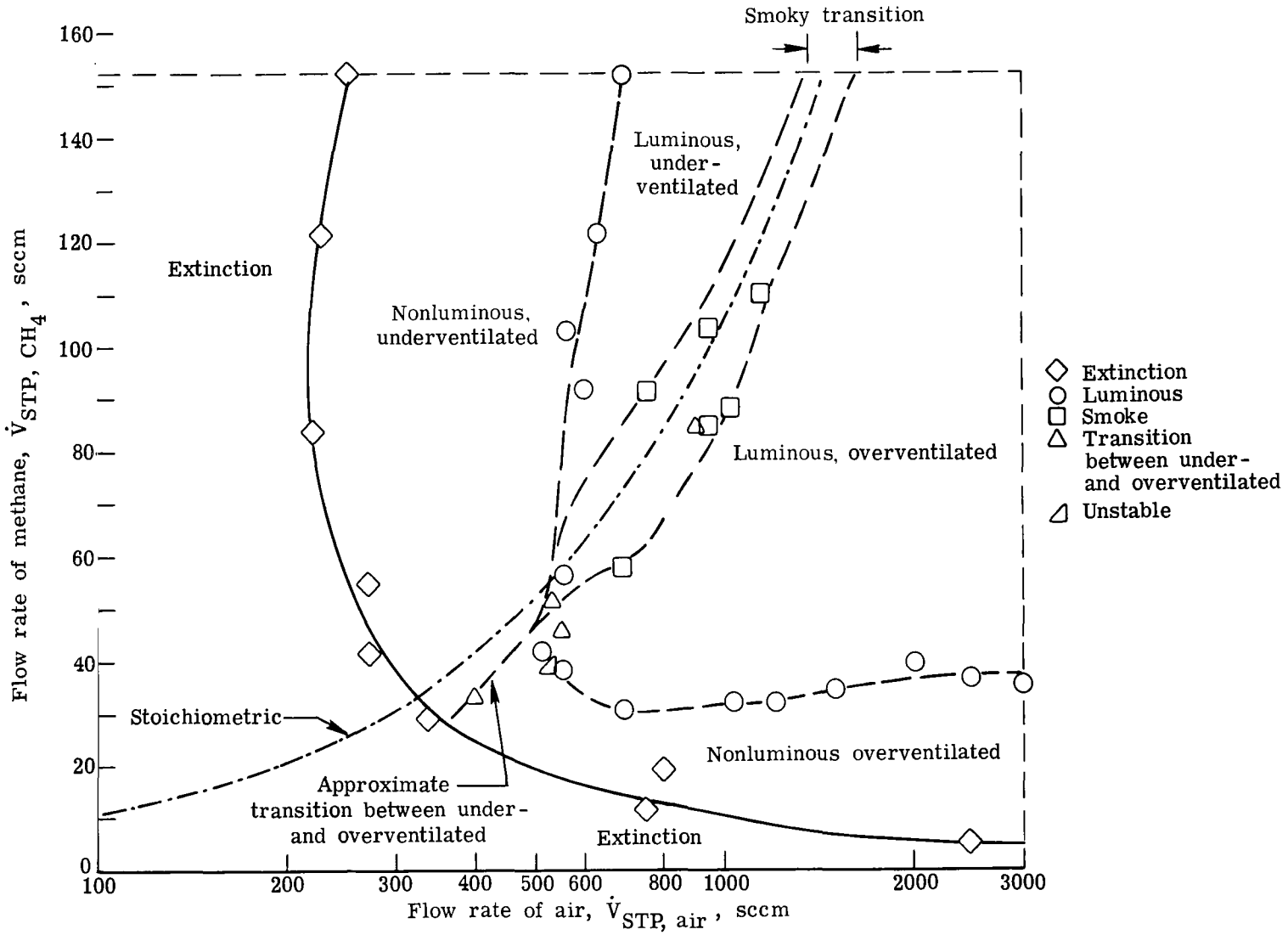

(a) p = 1 atm.

Figure 12.- Stability limits.

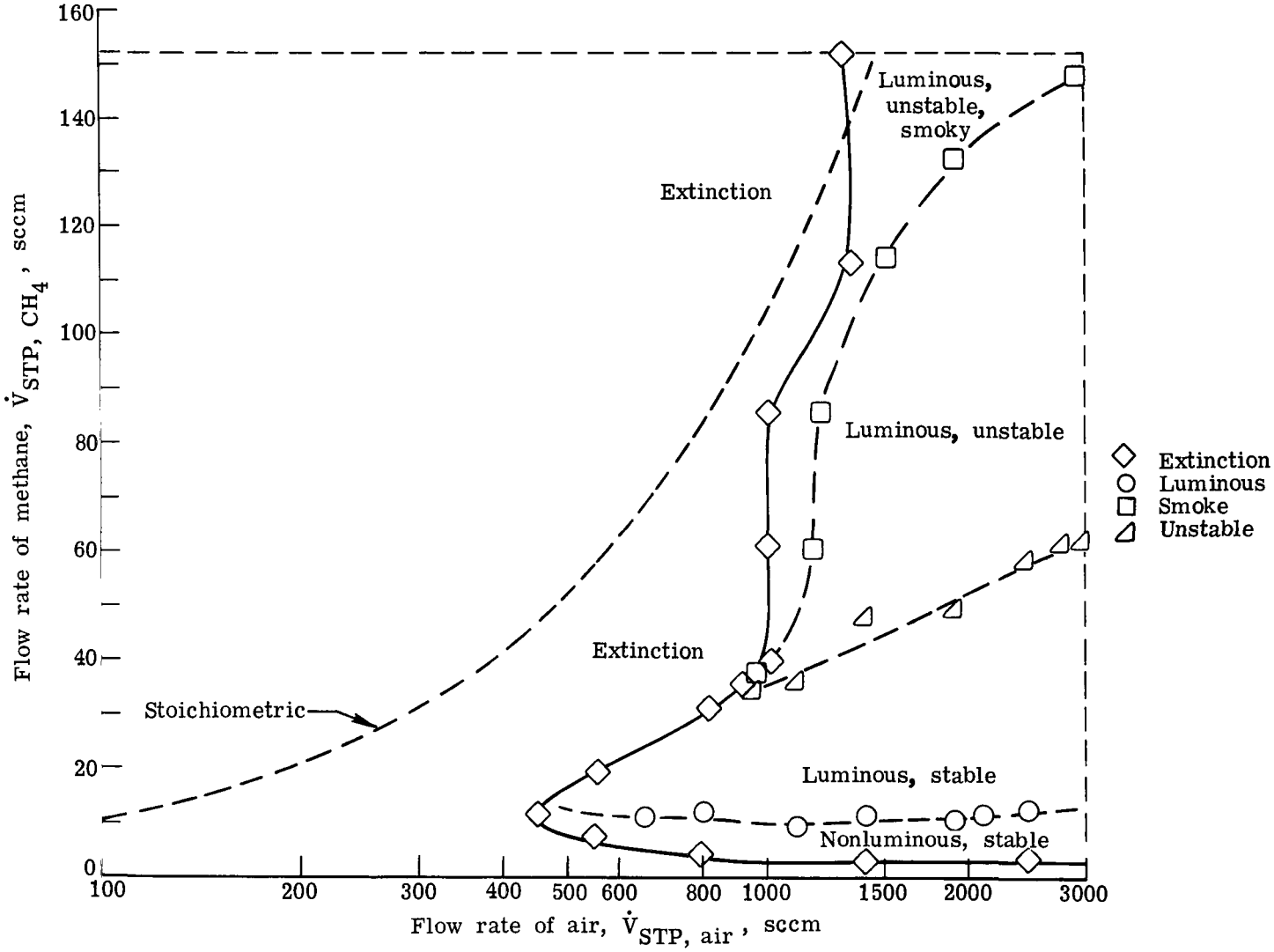

(b) p = 5 atm.

Figure 12.- Continued.

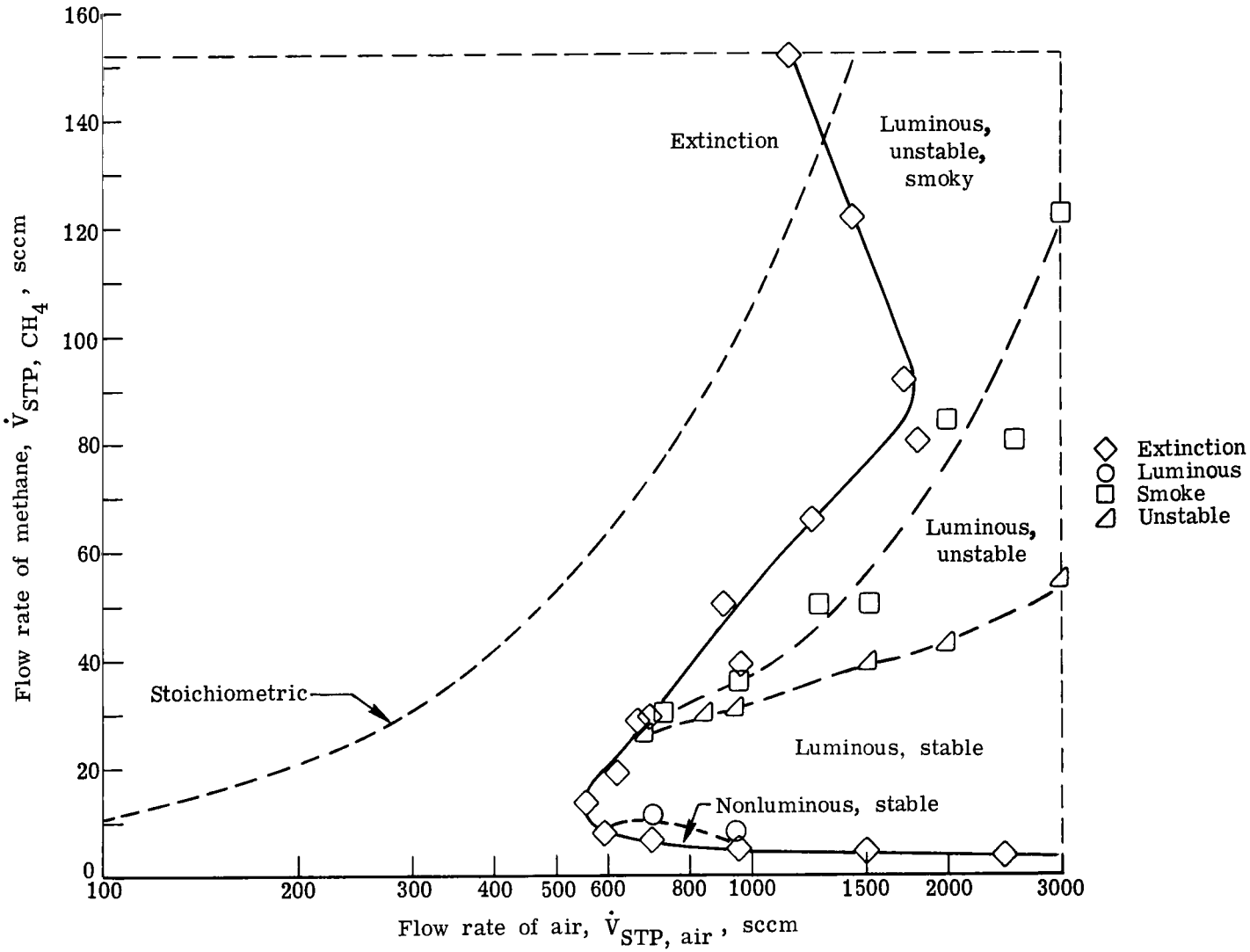

(c) p = 20 atm.

Figure 12.- Continued.

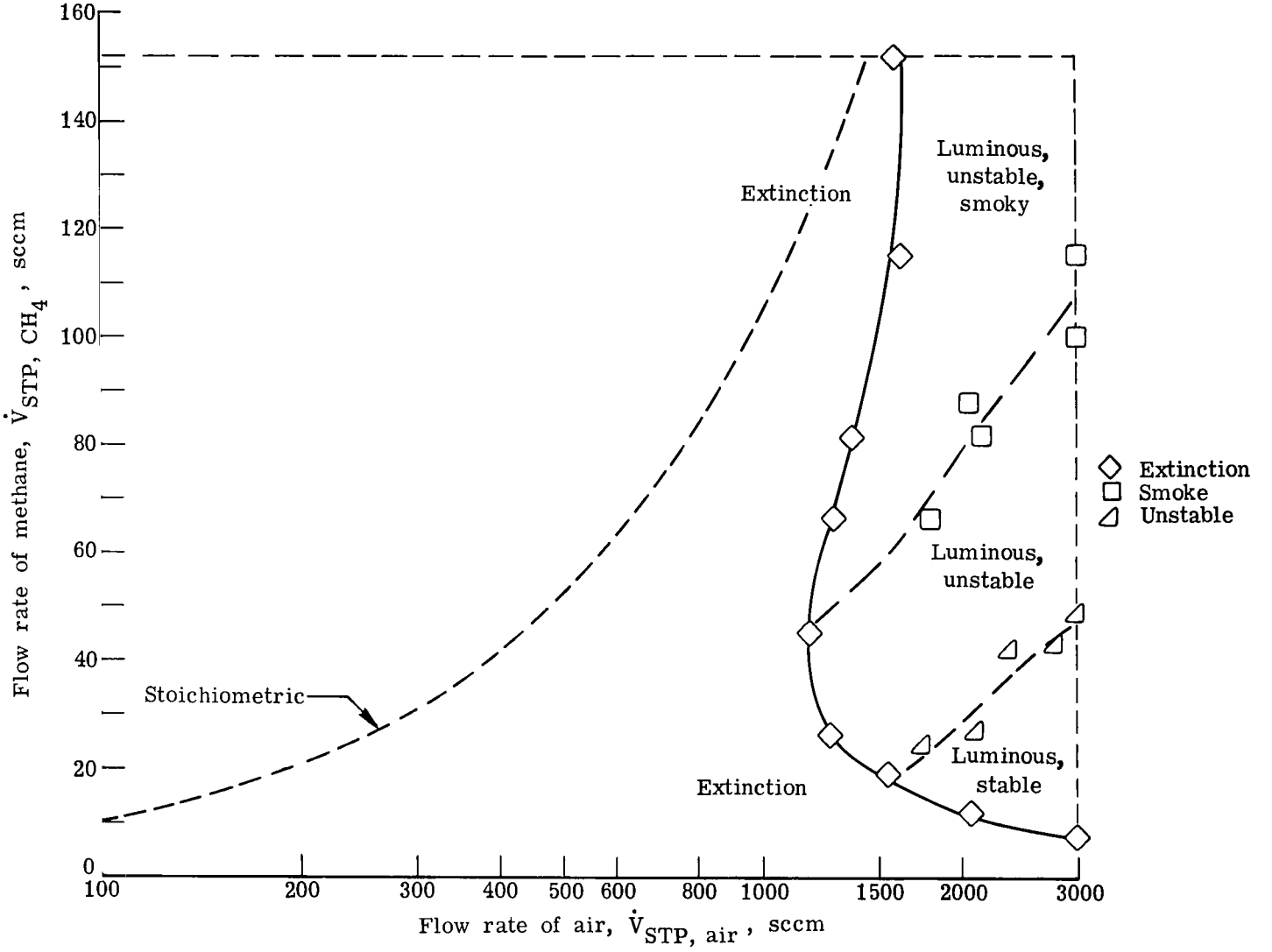

(d) p = 50 atm.

Figure 12.- Concluded.

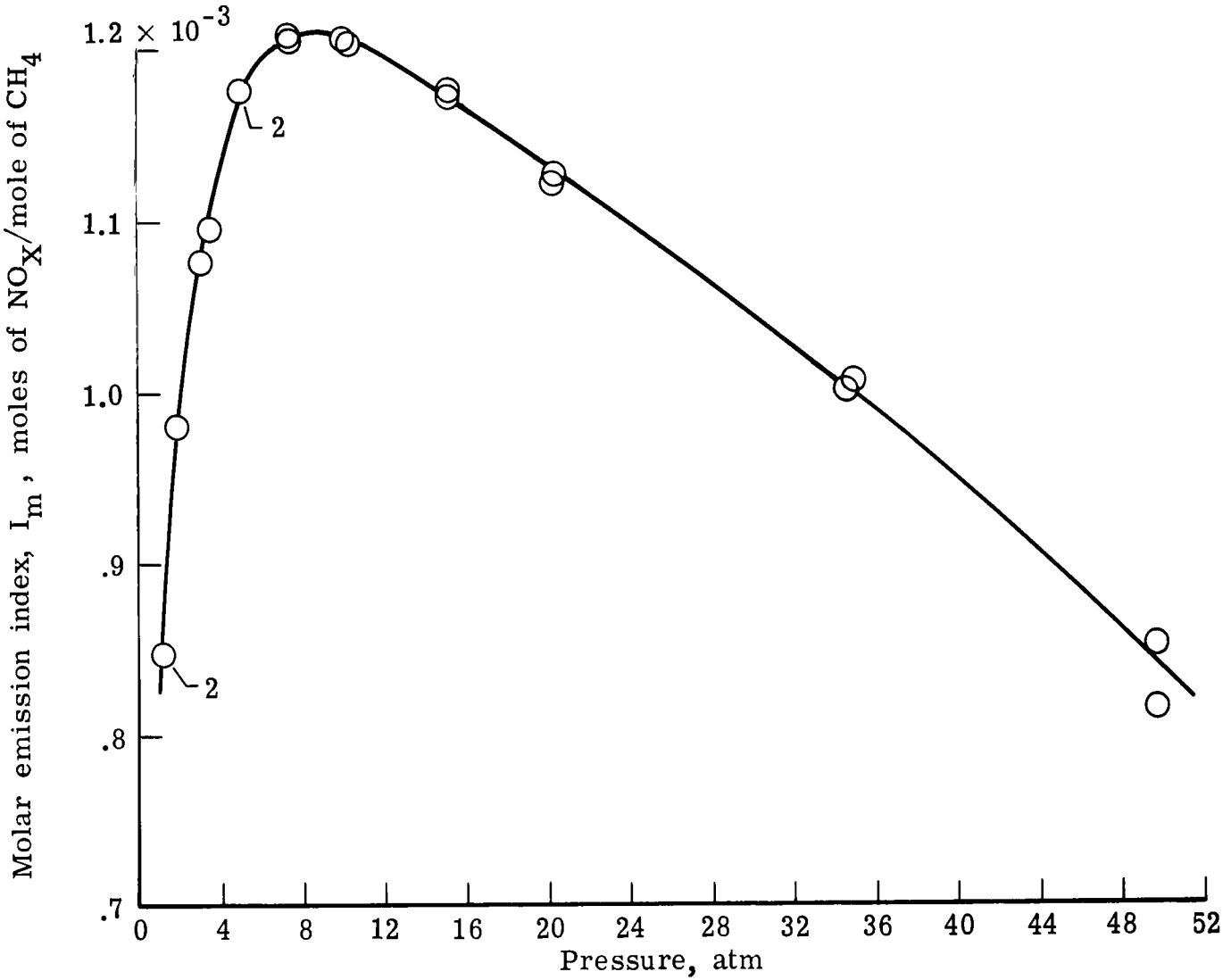

Figure 13.- Molar emission index of NO_x as function of pressure.

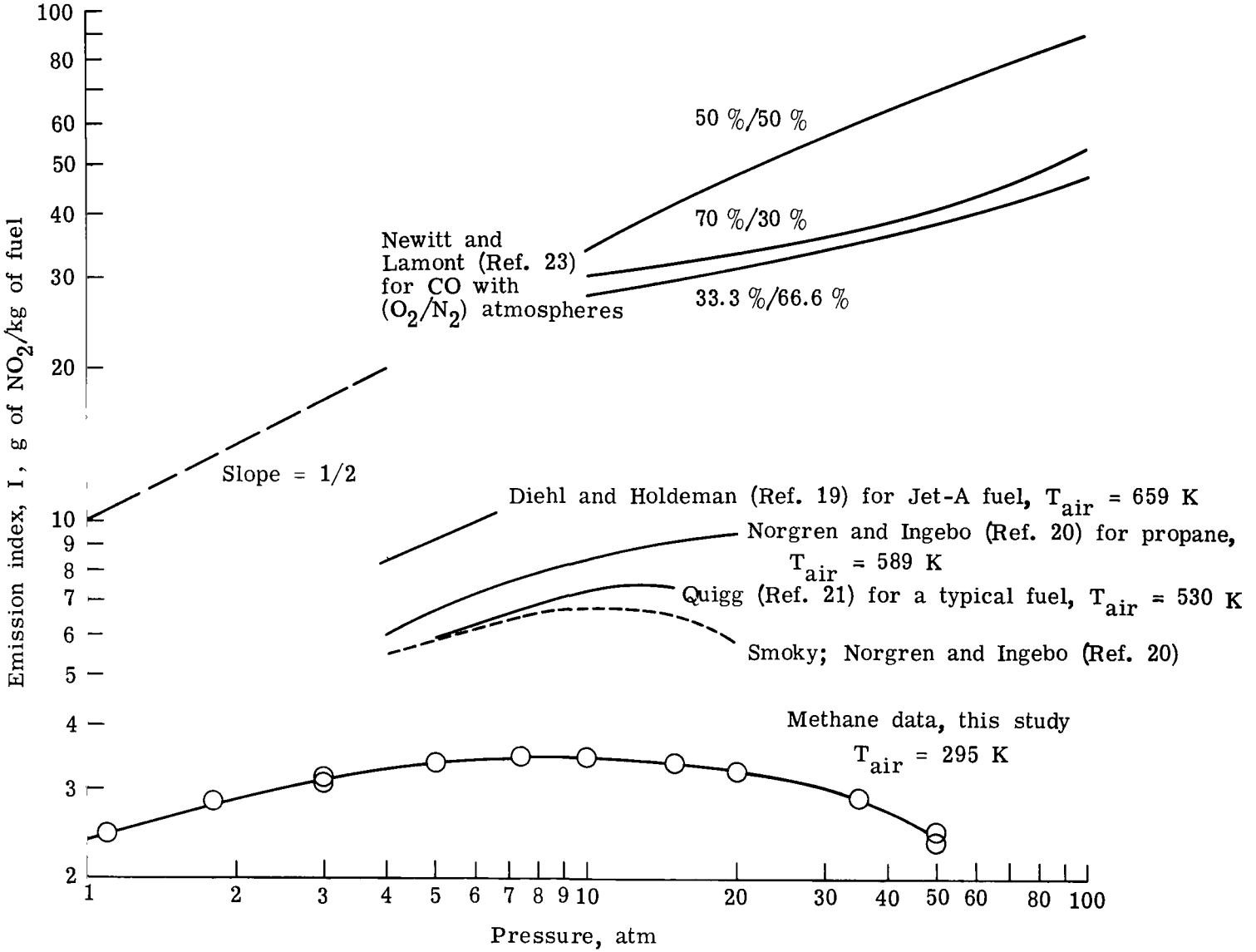

Figure 14.- Emission index as function of pressure.

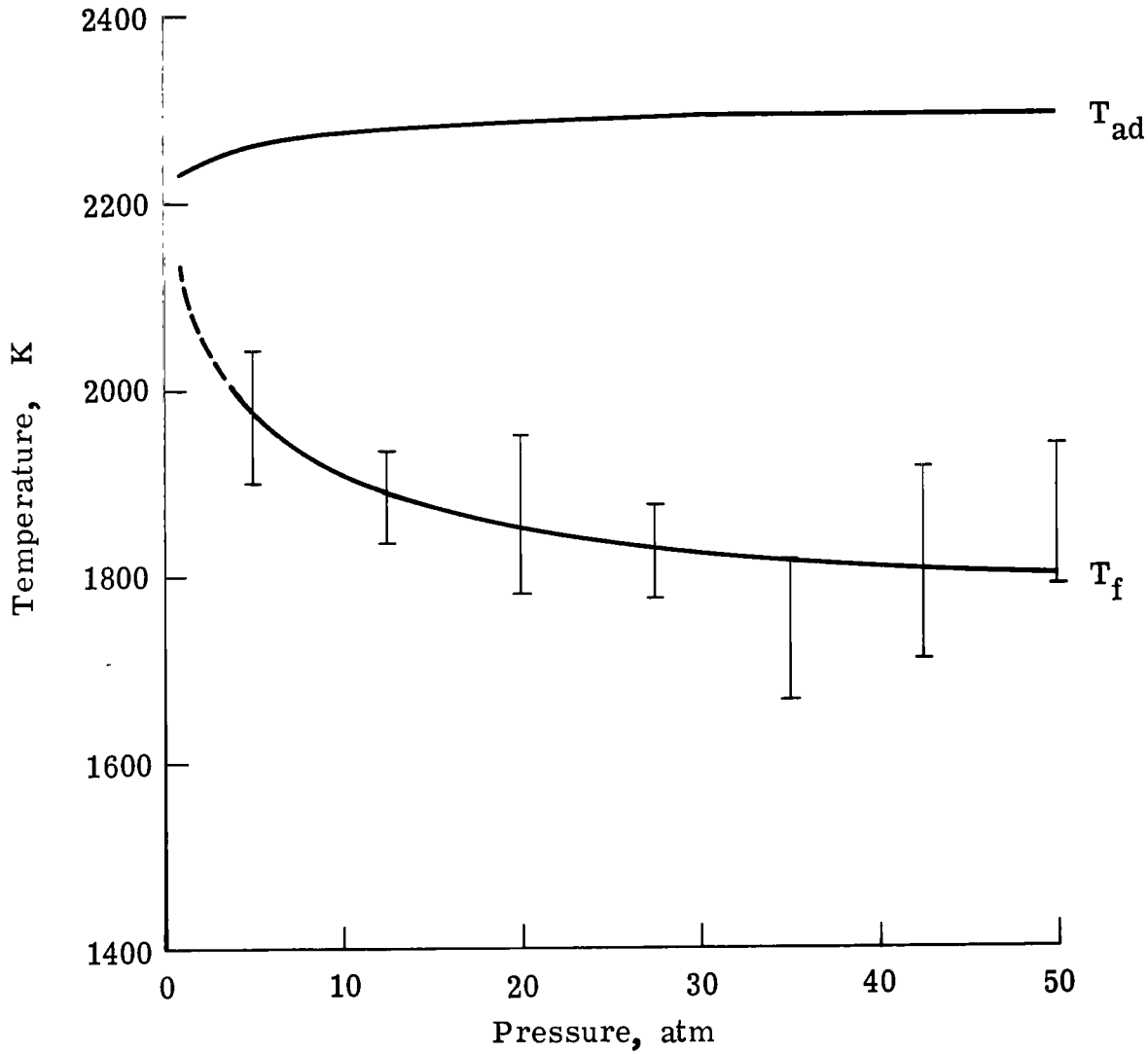

Figure 15.- Flame temperature as function of pressure.
Dashed line indicates extrapolation.

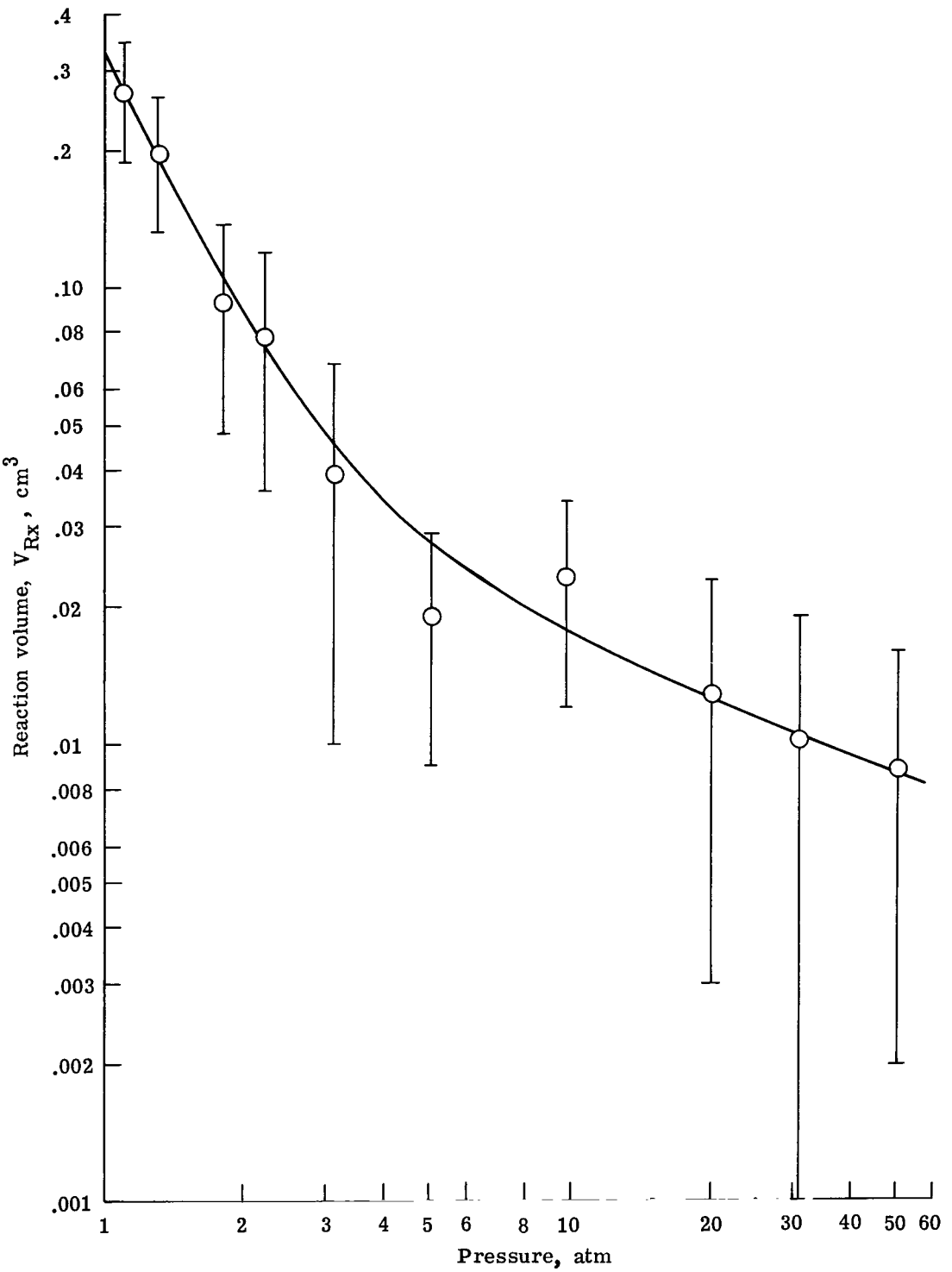

Figure 16.- Methane reaction volume as function of pressure.

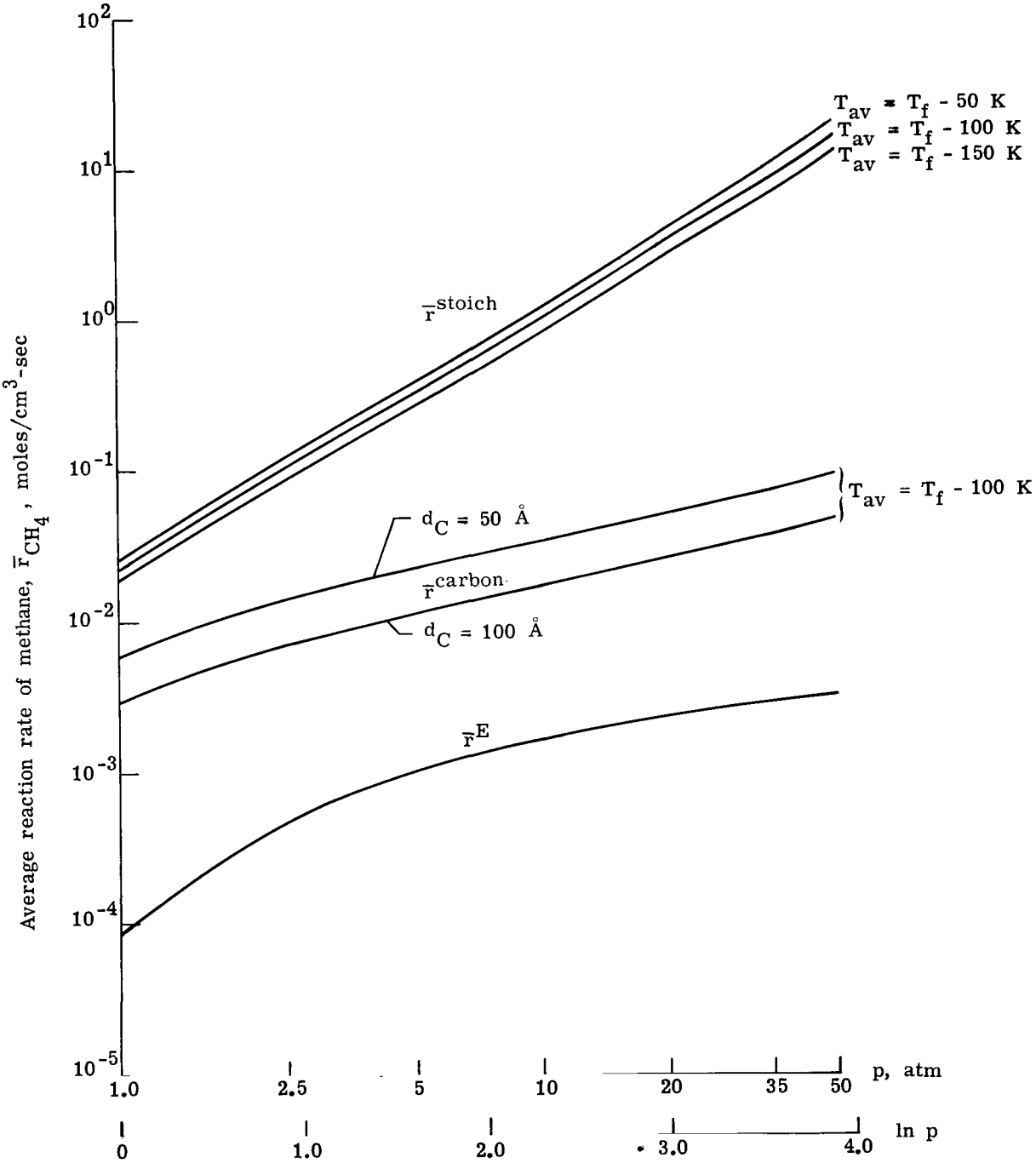

Figure 17.- Average methane reaction rate as function of pressure.

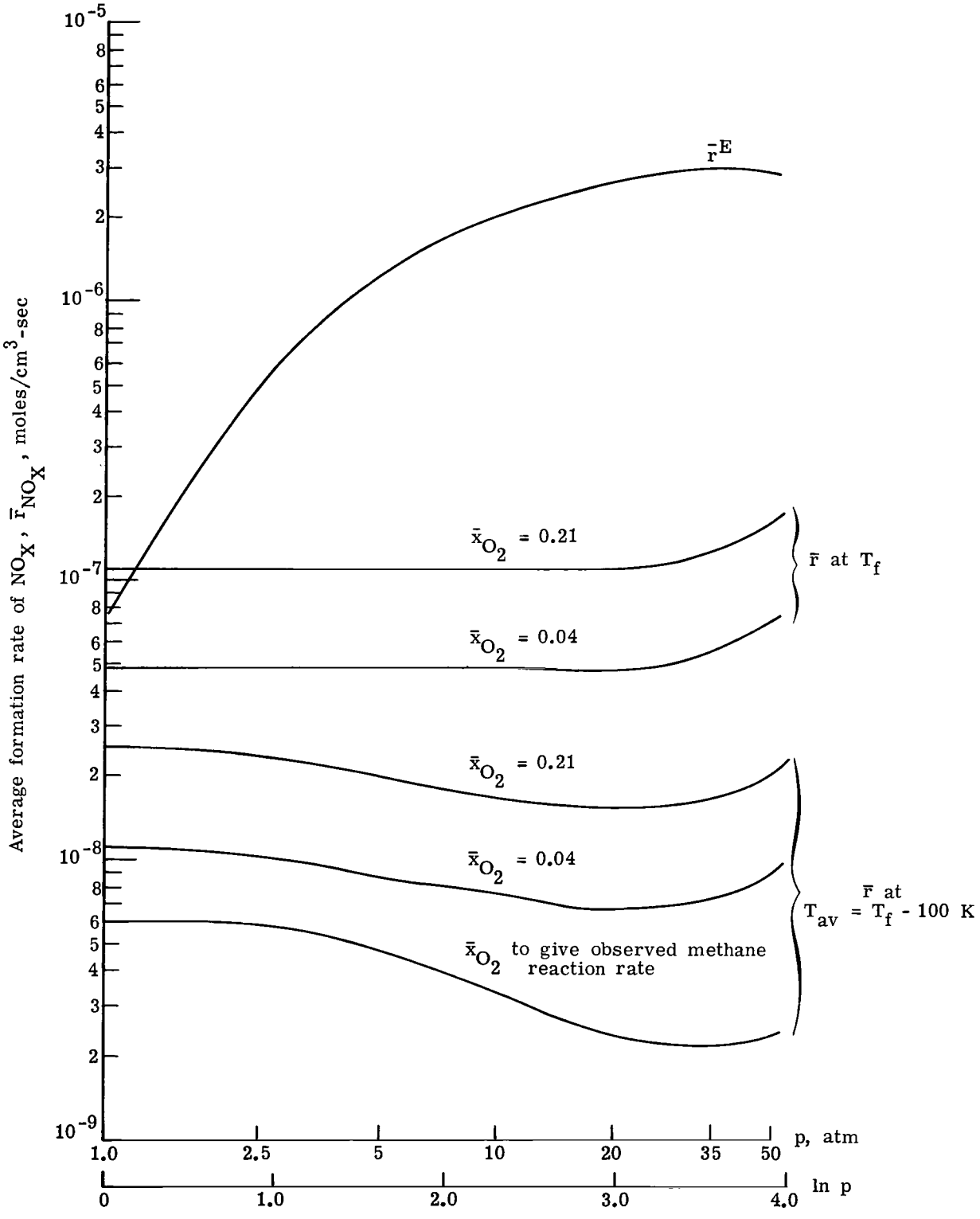

Figure 18.- Average NO_X formation rate as function of pressure.

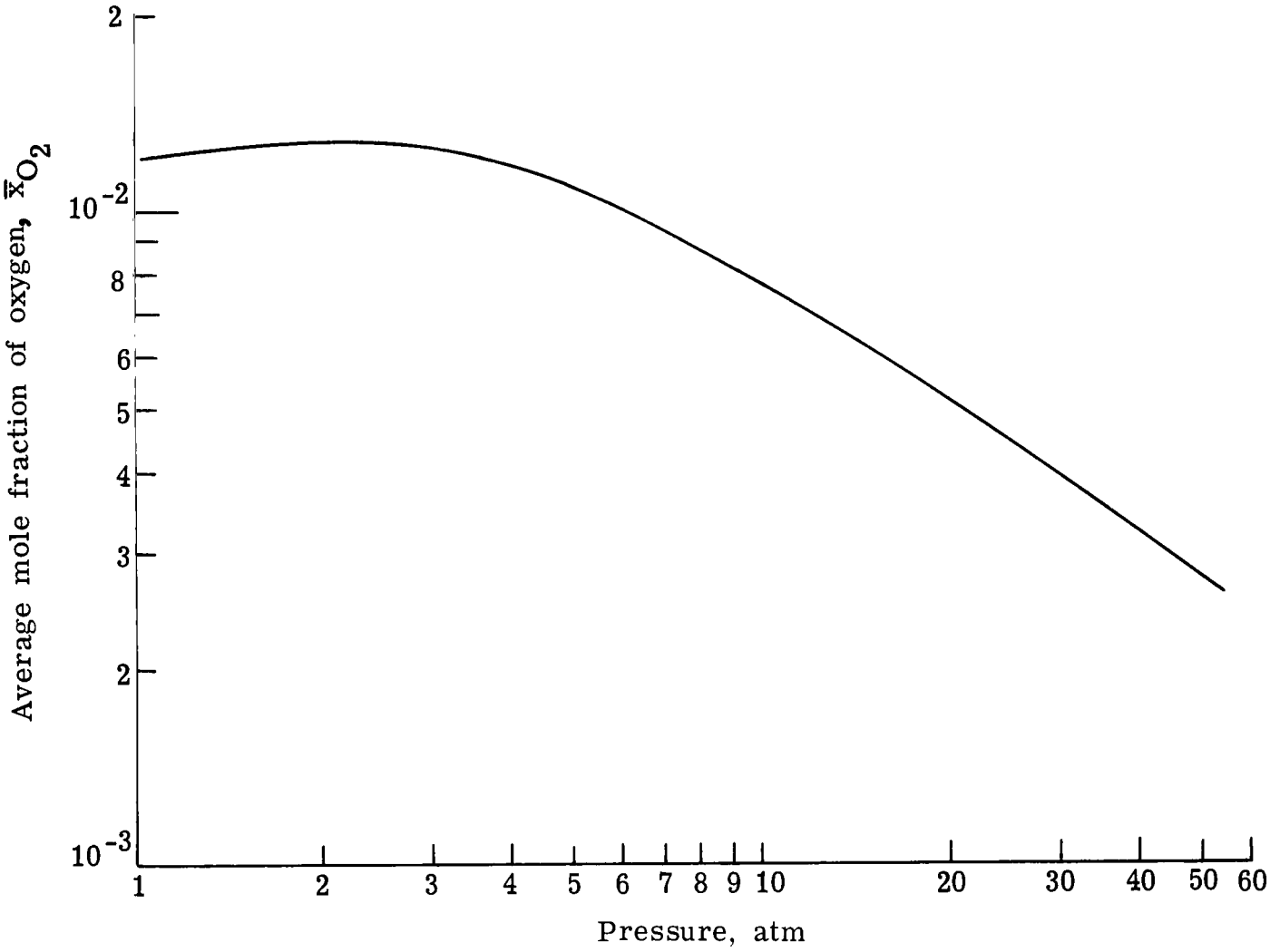

Figure 19.- Average mole fraction of oxygen to give observed methane reaction rate as function of pressure. $T_{av} = T_f - 100$ K.

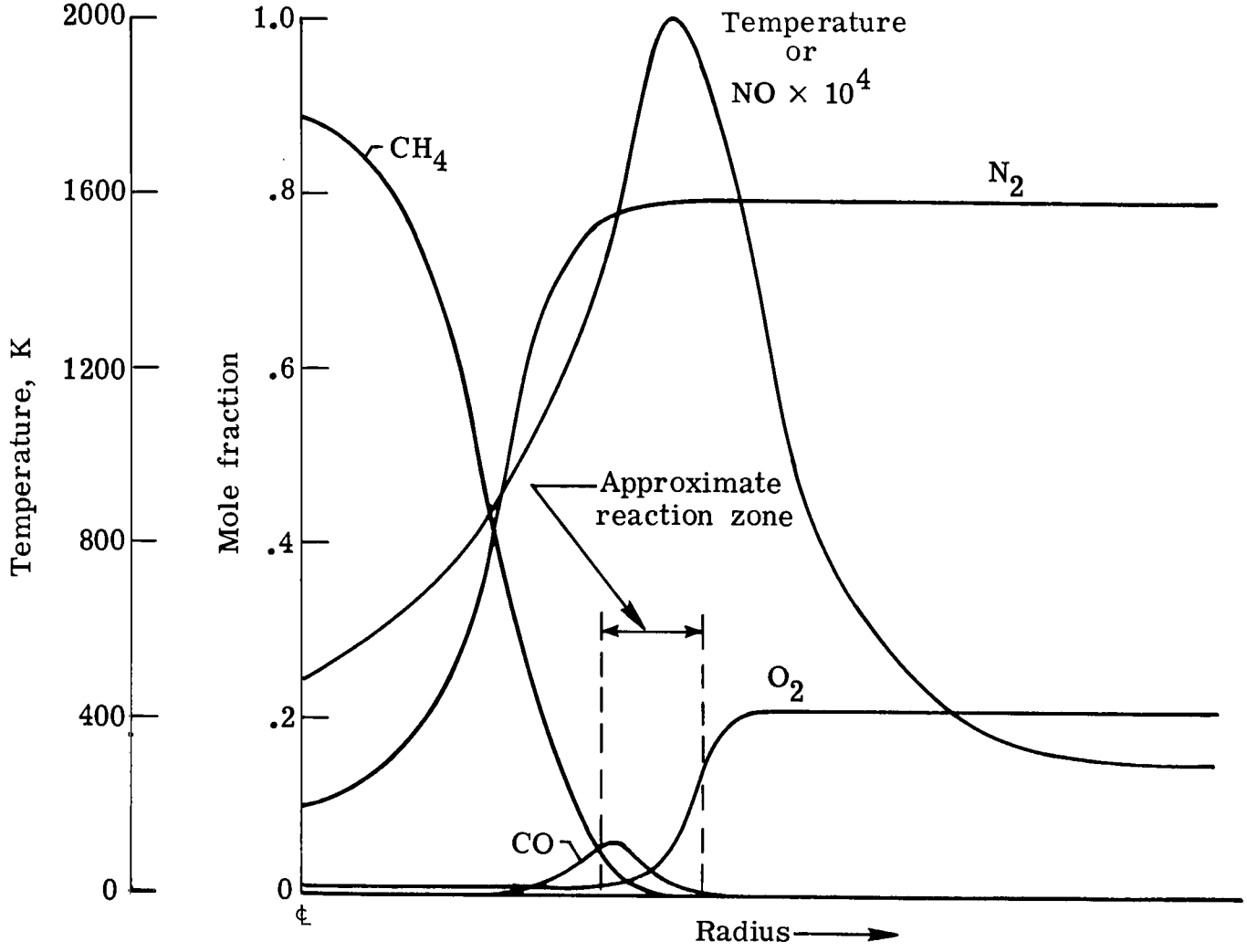

Figure 20.- Qualitative sketch of typical profile in a diffusion flame. Not all species are shown.

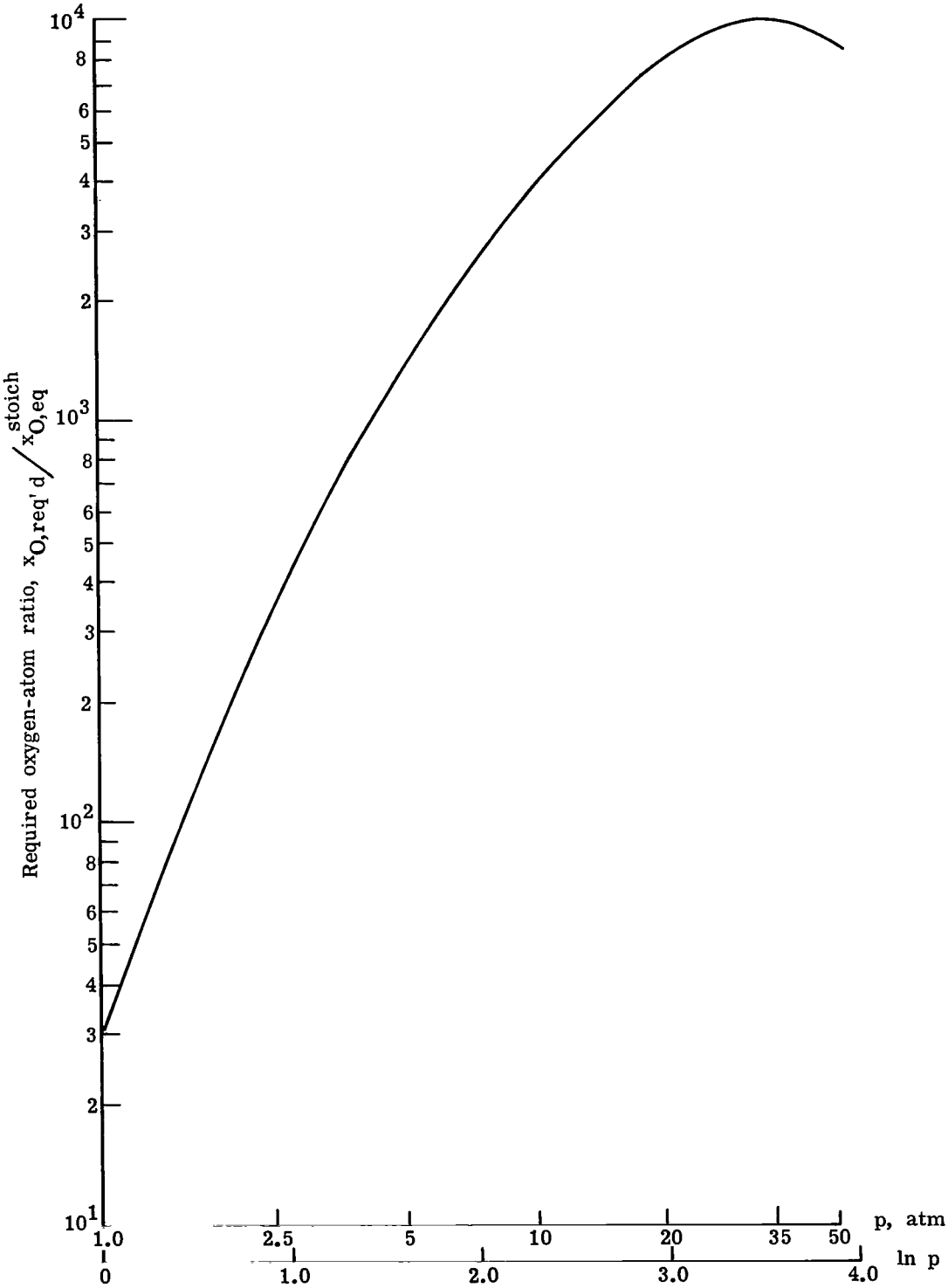

Figure 21.- Required oxygen-atom ratio as function of pressure. $T_{av} = T_f - 100$ K.

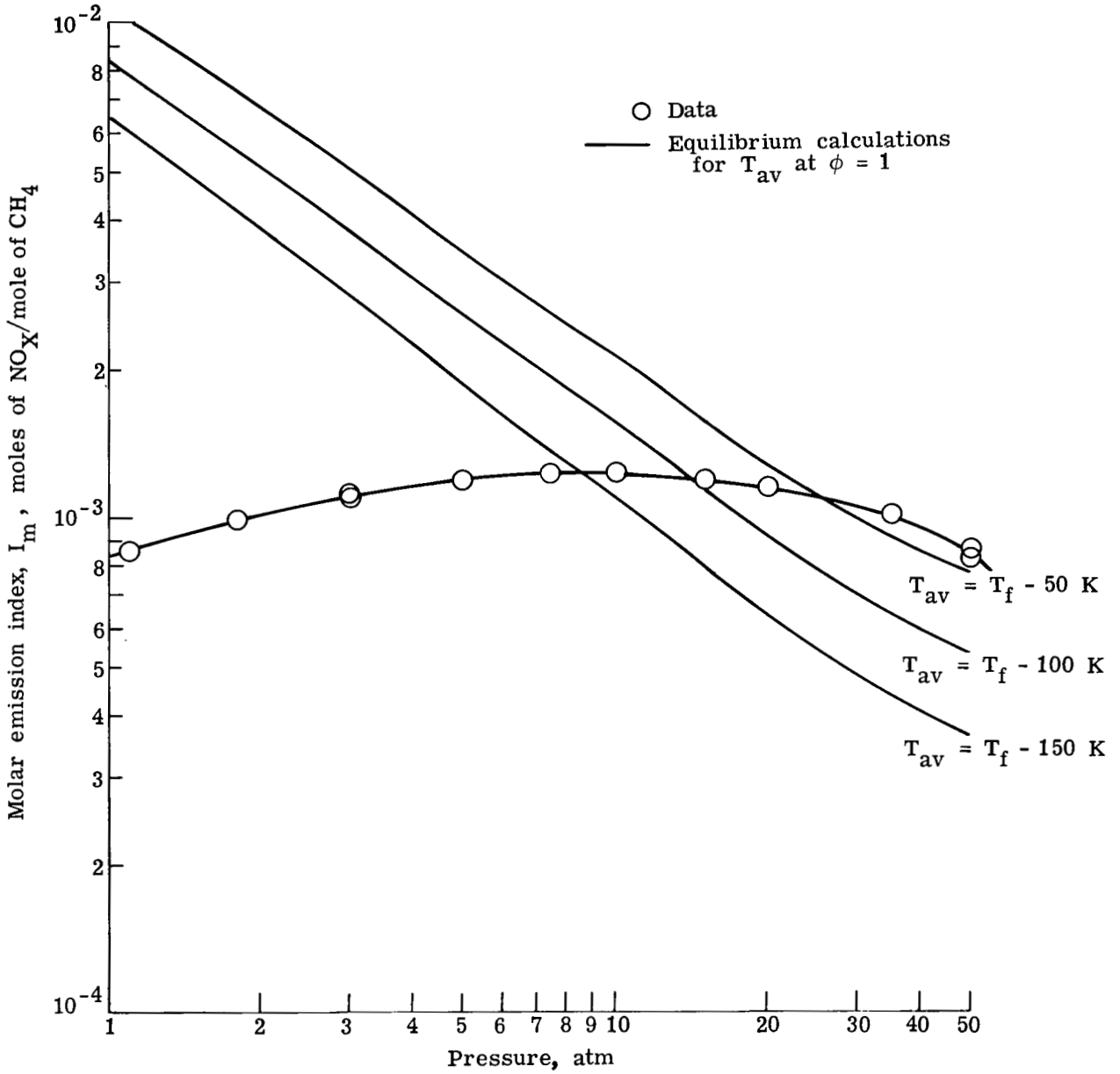

Figure 22.- Molar emission index as function of pressure.

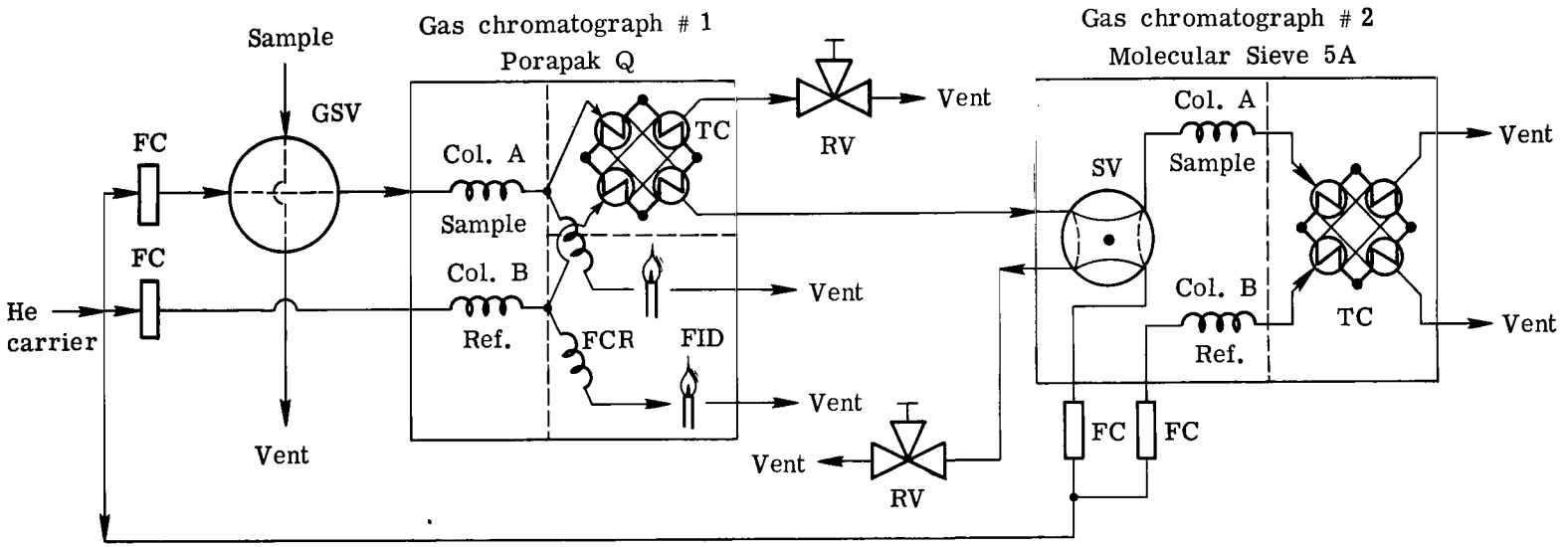

FC – Flow controller
GSV – Gas sample valve
RV – Regulating valve serving as adjustable restriction
SV – Switching valve
TC – Thermal conductivity cell
FID – Flame ionization detector
FCR – Fixed capillary restriction coil

Figure 23.- Gas chromatograph analytical train.

"The aeronautical and space activities of the United States shall be conducted so as to contribute . . . to the expansion of human knowledge of phenomena in the atmosphere and space. The Administration shall provide for the widest practicable and appropriate dissemination of information concerning its activities and the results thereof."

—NATIONAL AERONAUTICS AND SPACE ACT OF 1958

NASA SCIENTIFIC AND TECHNICAL PUBLICATIONS

TECHNICAL REPORTS: Scientific and technical information considered important, complete, and a lasting contribution to existing knowledge.

TECHNICAL NOTES: Information less broad in scope but nevertheless of importance as a contribution to existing knowledge.

TECHNICAL MEMORANDUMS: Information receiving limited distribution because of preliminary data, security classification, or other reasons. Also includes conference proceedings with either limited or unlimited distribution.

CONTRACTOR REPORTS: Scientific and technical information generated under a NASA contract or grant and considered an important contribution to existing knowledge.

TECHNICAL TRANSLATIONS: Information published in a foreign language considered to merit NASA distribution in English.

SPECIAL PUBLICATIONS: Information derived from or of value to NASA activities. Publications include final reports of major projects, monographs, data compilations, handbooks, sourcebooks, and special bibliographies.

TECHNOLOGY UTILIZATION PUBLICATIONS: Information on technology used by NASA that may be of particular interest in commercial and other non-aerospace applications. Publications include Tech Briefs, Technology Utilization Reports and Technology Surveys.

Details on the availability of these publications may be obtained from:

SCIENTIFIC AND TECHNICAL INFORMATION OFFICE

NATIONAL AERONAUTICS AND SPACE ADMINISTRATION

Washington, D.C. 20546